AMERICAN UNIVERSITY OF BEIRUT

DEGRADATION OF SULFAMETHOXAZOLE ANTIBIOTIC IN MIL88-A/PS SYSTEMS: IMPLICATION OF SOLAR IRRADIATION FOR PROCESS IMPROVEMENT

by
ZAHRAA HUSSEIN ABOU KHALIL

A thesis
submitted in partial fulfillment of the requirements
for the degree of Master of Science
to the Department of Chemistry
of the Faculty of Arts and Sciences
at the American University of Beirut

Beirut, Lebanon
February 2021

AMERICAN UNIVERSITY OF BEIRUT

DEGRADATION OF SULFAMETHOXAZOLE ANTIBIOTIC IN
MIL88-A/PS SYSTEMS: IMPLICATION OF SOLAR
IRRADIATION FOR PROCESS IMPROVEMENT

by
ZAHRAA HUSSEIN ABOU KHALIL

Approved by:

_____
Dr. Antoine Ghauch, Full Professor   Advisor
Department of Chemistry

_____
Dr. Mohamad Hmadeh, Associate Professor   Member of Committee
Department of Chemistry

_____
Dr. Kamal Bouhadir, Full Professor   Member of Committee
Department of Chemistry

Date of thesis/dissertation defense: February 17, 2021

AMERICAN UNIVERSITY OF BEIRUT

THESIS RELEASE FORM

Student Name: ___Abou Khalil_____Zahraa_____Hussein_____
                            Last   First   Middle

I authorize the American University of Beirut, to: (a) reproduce hard or electronic copies of my thesis; (b) include such copies in the archives and digital repositories of the University; and (c) make freely available such copies to third parties for research or educational purposes:

☐ As of the date of submission

☐ One year from the date of submission of my thesis.

☐ Two years from the date of submission of my thesis.

☒ Three years from the date of submission of my thesis.

_____

Signature   Date: February 27, 2021

ACKNOWLEDGMENTS

First and foremost I would like to express my gratitude to my thesis supervisor and mentor Dr. Antoine Ghauch for his endless patience, motivation and support throughout my research work at AUB. Dr. Ghauch was always available to guide me and answer my questions throughout all my research experience.

 Moreover, I'm thankful to the members of this committee: Dr. Kamal Bouhadir and Dr. Mohamad Hmadeh for their beneficial comments and feedback.

A special thanks goes to Dr. Hmadeh research group for their imput in the characterization of MIL88-A especially Ghewa El Sabeh.

We are also very thankful to Dr. Mario El Kazzi, group leader in the electrochemical Energy Storage Section at Paul Scherrer Institute for performing and interpreting the XPS analysis and to Dr. Maxim Yilkov who helped in performing the EPR analysis and simulations at ETH, Switzerland.

In addition to that, a perfect work requires the effort of a group of people. This is achieved by the American University of Beirut (AUB) which gave us the opportunity to receive quality learning as well as the opportunity to work with the most developed machines to accomplish our experimental work. Special thanks go to the academic and nonacademic staff of the Chemistry department and to the staff of the KAS CRSL for their effort in maintaining the flow of the research work.

Furthermore, I would like to thank my lab mates Abbas, Suha, Maya, Rime, Sarah, and Omar for keeping an ideal work place environment and teaching me all what I need for the research work.

Thank you my dear friends Ghewa, Fairouz, Salah, Zeinab, Meghrie, Rawan and Manal for all the support and help throughout my three years journey. Because of you, AUB was a second home.

Finally, no words can express my gratitude to my family for always being there for me. I wouldn't have accomplished my goals without their endless love, support and motivation.

ABSTRACT
OF THE THESIS OF

Zahraa Hussein Abou Khalil   for   Master of Science
                                                          Major: Chemistry

Title: Degradation of Sulfamethoxazole Antibiotic in MIL88-A/PS Systems: Implication of Solar Irradiation for Process Improvement

PPCPs, a class of emerging contaminants poses significant negative impacts on the ecosystem and possibly on human health. Sulfamethoxazole (SMX), an antimicrobial agent, has been detected, at trace concentrations, in surface water around the globe. One of the main entry routes of SMX is its discharge from pharmaceutical production plants. AOPs are the established methods for the elimination of high concentration of hazardous organic compounds, in an aqueous matrix, such as SMX. PS-based AOPs have shown, over the last 10 years, to be the most efficient and sustainable alternative to H_2O_2 based AOPs. PS can be activated by several methods, the simplest is the homogenous chemical activation by ferrous ions. The pursuit for new candidate activating agents that require fewer chemicals and are easily separated from the bulk solution is important for developing PS-based AOPs. Metal Organic Frameworks (MOFs), a relatively new class of porous 3d material, are being researched for their applications in environmental remediation and waste water treatment. MIL-88-A, an iron based MOF (Fe^{3+}/Fumaric acid), is synthesized in aqueous medium, a greener advantage over other MOFs that require organic solvents. The aim of the project is to characterize MIL-88-A and to test its capability to act as an assisting agent for the elimination of PPCPs from waste water using AOPs. A solution containing SMX, was placed in continuously stirred reactors, irradiated with two commercial UVA lamps or solar irradiation and finally spiked with PS and MIL-88-A consecutively. The study shows the combined effects of UVA or solar /MIL88-A/PS as well as the effect of various factors such as MOF load, and matrix effect. It also investigates the activation mechanism, its effectiveness, recyclability of MIL-88-A. R. Total degradation of SMX ($[SMX]_0 = 5$ ppm) occurred in a period of two hours using a system of UVA/MIL-88-A/PS and complete degradation occurred in 5-20 minutes in a system of Solar/MIL-88-A/PS.

Keywords: MOF, AOPs, Sulfamethoxazole, MIL88-A, persulfate

TABLE OF CONTENTS

ILLUSTRATIONS

Figure

TABLES

ABBREVIATIONS

Abbreviation	Meaning	Page
AOPs	Advanced oxidation processes	12
BP1	Byproduct one	54
BP2	Byproduct two	54
BP3	Byproduct three	54
HRs	Hydroxyl radicals	12
MOFs	Metal-organic frameworks	13
PPCPs	Pharmaceutical and personal care products	11
PS	Persulfate	12
SMX	Sulfamethoxazole	17
SRs	Sulfate radicals	12
WWTPs	Wastewater treatment plants	11

CHAPTER 1

INTRODUCTION

1.1 PPCPs as emergent contaminants

Pharmaceuticals and personal care products (PPCPs) are a group of various organic and inorganic compounds. These materials include antibiotics, hormones, antimicrobial agents, NSAIDs, cosmetics, fragrances, etc. They were classified as emerging environmental contaminants in the last two decades due to their environmental and potential human health risks. [1–3]. Many research projects were conducted to study the effect of PPCPs not only on the aquatic environment but also on the terrestrial one including their presence, magnitudes, factors that affect their levels, consequences, and treatment [1]. Their increasing levels were attributed to the growing human population as well as the increase in life expectancy. For instance, human population has been increasing at an alarming pace, with a notable rise in men's age and the global growth in the demand of meat and dairy products has expanded the global animal population needing the use of pharmaceutical products [4]. PPCPs tend to enter the environment through different routes. Human and animal wastes is one of the main routes. In addition to the uncontrolled disposal of expired medications into the waste water or landfills which may reach surface and ground water as well as soil. Similarly. industrial effluents proved to contain considerable amounts of these PPCPs [5,6]. Several studies proved that the conventional waste water treatment plants (WWTPs) are not efficient for the complete elimination of PPCPs due to their stability and resistance to change [5]. WWTPs is mainly based on

adsorption followed by degradation of these compounds. However, a large class of PPCPs known as nonsteroidal anti-inflammatory drugs (NSAIDs) have pKa values ranging between 4,1 and 4.9, and thus they exist as ions at surface water of neutral pH, making them more resistant to elimination. Then comes biodegradation which requires high cost, high sludge age and retention time[7]. For example, the efficient elimination of Diclofenac was only attained when the sludge age was at least 8 days [3].PPCPs are mainly made of two components: excipients and active pharmaceutical ingredients (APIs). The presence of APIs in waste water plants had been stated, in many counties over the world, in the levels of ng L^{-1} to µg L^{-1} [2], such as US [8], UK [9], Spain [10], Finland [11], and Japan [12]. The resistance of PPCPs to the available treatment methods led to the accumulation and possibly the bioamplification of the pharmaceuticals in water which possess a significant negative impact on the ecosystem and possibly on human health [13]. For instance, many studies proved that antibiotics might subsidize the growth of multi-drug resistant bacteria, which in turn causes a major challenge in the medical community [14]. Over the last two decades, these categories of PPCPs have been widely used due to their low cost, availability over the counter and minor side effects. Consequently, significant concentrations of these pharmaceuticals and their metabolites reach groundwater, and even surface and drinking water [15,16].

1.2 Advanced oxidation processes AOPs

As conventional waste water treatment methods have been proven to be insufficient for the complete removal of some recalcitrant pharmaceuticals, it was necessary to search for advanced treatment technologies. One of which is advanced oxidation processes (AOPs).

AOPs are extensively studied and applied for industrial waste water treatment and are considered the most effective techniques for the removal of low and high concentrations of organic contaminants that cannot be totally eliminated by conventional WWTPs [17]. They are based on the use of highly reactive species, mainly hydroxyl radicals (HRs), in oxidative mechanisms leading to the complete degradation of the target compounds [18]. Common AOPs include ozonation, UV-based processes (UV/H_2O_2, UV/H_2O_2/O_3, etc.) ,Fenton reaction (Fe^{2+}/H_2O_2) and persulfate based AOPs are currently used in industrial WWTPs [19–21]

1.3 Persulfate based AOPs and its activation methods

Persulfate (PS) based AOP is being widely used in the past years due to the variety of activation mechanisms that can be applied for PS [22], being a cost-effective method compared to other AOPs [11], and being an environmental friendly method whereby it degrades pharmaceuticals into sulfate ions in aqueous medium. [23]. Upon its activation, PS ($E_0 = 2.1$ V) generates highly reactive sulfate radicals (SRs) ($E^0 = 2.6$ V) characterized by a longer lifetime (t = 20-30 µs) compared to hydroxyl radicals (HRs) ($E^0 = 2.7$) that are relatively very reactive with half-life equals 10^{-9} s [24–26]. SRs are characterized by being very reactive against organic contaminants, since they are non-selective and have a high oxidizing ability across a broader range of pH compared to HRs radicals [27]. The most common PS activation methods are thermal (Eq. 1) [28–30], UV (Eq. 2) [31–33] and chemical using Fe^{2+} ions in homogeneous medium (Eq. 3) [34,35] or heterogeneous catalyst such as MOFs or magnetite [36,37]. We are interested in the application of MOFs especially those containing iron as transition metal.

$$S_2O_8^{2-} \rightarrow 2\ SO_4^{-\bullet} \quad \text{(Thermal activation) with } 30^o\ C\ < T < 99^o \tag{1}$$

$$S_2O_8^{2-} \xrightarrow{h\upsilon} 2\ SO_4^{-\bullet} \quad \text{(UV activation)} \tag{2}$$

$$S_2O_8^{2-} + Fe^{2+} \rightarrow SO_4^{2-} + SO_4^{-\bullet} + Fe^{3+} \quad \text{(Chemical activation)} \tag{3}$$
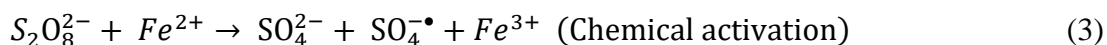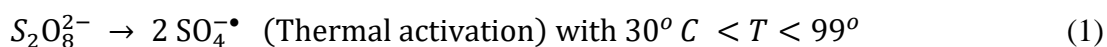
1.4 Metal organic frameworks (MOFs): definition and properties

MOFs are a relatively new class of porous 3d materials. They have a modular structure that gives them huge structural diversity and the possibility of creation of materials with tailored characteristics. They are synthesized through different methods such as microwave, ultrasonication, electrochemical and mechanochemical processes. It is important to mention that, the reproducibility in the results of the synthesis procedures is a crucial factor that must be followed up. MOFs are also functionalized so that they suite certain applications. They consist of metal ions or clusters connected to organic linkers to form one, two, or three-dimensional structures. In the past, MOFs were defined as a subclass of coordination polymers, with the special property of being highly porous. This has changed upon discovering that the inorganic part has high dimensionality that can form layers and may extend to frameworks and not only chains [39,40]. This combination of organic and inorganic structure leads to materials with unique properties, as so MOFs are often characterized by their high surface area reaching around 10,000 m^2/g, and huge pore volumes around 50 % of the total volume or more (0.99 $cm^3g^{-1}10^{-2}$ for MIL88A) [41,42]. These properties make them good candidate for gas adsorption or separation [43–45], drug delivery [46,47], magnetism [48], polymerization [49], catalysis [50], and many other applications.

1.5 Use of MOFs in adsorption processes

MOFs having metal ions such as Ti, Zr, Fe, Al and/or Cr with carboxylate-based ligands are mainly stable in water and have been widely used in adsorptive applications of hazardous organic compounds in waste water [40,51–53]. For instance, Haque et al. studied the removal of methyl orange (MO), a toxic anionic dye from aqueous solutions using MIL-101-Cr. Results showed good adsorption capacity (114 mg/g) [51]. However, this study presents certain drawbacks starting with chromium which is a toxic metal especially in the hexavalent state [54]. Moreover, MIL-101 was synthesized using hydrofluoric acid which is not recommended when dealing with environmental applications since it is highly toxic and corrosive [55]. Furthermore, MIL-100-Fe was used in various adsorption application with different research groups such as Tomg et al., Huo et al. and Hasan et al. for the removal of MO, malachite green (MG) and naproxen respectively [56–58]. All the above-mentioned studies showed that adsorption alone is insufficient for the removal of trace amounts of the stated PPCPs. In addition to that, arsenic adsorption to MIL-53-Fe was investigated by Vu et al. for its elimination from aqueous solution. The adsorptive mechanism was based on Lewis acid-base interaction between the anionic $H_2AsO_4^-$ species and the MOF node which renders it selective for a specific range of adsorbents [59]. For more clarification, Gao et al. studied the adsorption of carbamazepine (CPZ), a pharmaceutical that is used for the treatment of epilepsy and proved to have a high environmental risk, on MIL53 (Cr) for its removal from aqueous medium. Results showed that the chemisorption of CPZ to the MOF was predominant allowing its elimination [60].

1.6 The use of MOFs in catalysis

Other than adsorption, MOFs, especially those having Fe as a metal ion, showed effective photo catalytic activity for the removal of organic pollutants. This activity is accomplished by the use of a mediator such as PS. Recently, Fe based MOFs have been investigated for the activation of PS to degrade organic dyes [61,62]. Experiments showed promising results especially in recyclability and reproducibility rendering MOFs a greener alternative [63]. For example, Li et al. studied the degradation of acid orange 7 (AO7) by activating PS using four different MOFs [63]. The results showed that MIL-101 (Fe) has the best adsorption properties and catalytic activity toward PS activation for the removal of AO7 [63]. Furthermore, Hu et al. demonstrated the degradation of organophosphorus flame retardant, tris(2-chloroethyl) phosphate (TCEP) [64]. The mechanism of photo-catalysis is mainly based on the transformation of Fe(III) into Fe(II) (eq. 4), after which PS is transformed to sulfate radicals (Eq. 3), allowing the degradation of TCEP to occur by free radical mechanism (Eq.5) as proposed in their research, as well as other studies using iron-based MOFs [64].

$$\equiv Fe^{3+} \xrightarrow{irradiation} \equiv Fe^{2+} \tag{4}$$

$$SO_4^{-\bullet} + \text{contaminant} \rightarrow \text{byproducts} \tag{5}$$

For example, MIL-53 (Fe) was used by Pu et al. for the degradation of orange G (OG) in water. Altered synthesis procedures under different time and temperature were demonstrated, however no significant influence on the structure of MOFs was observed. Results also showed that MIL-53(Fe) can't totally progress at a temperature less than

150˚C. OG was fully degraded under optimal conditions within 90 min and the COD

removal reached a rate of 74% after 120 min [65]. Also, Li et al. studied the degradation of

dibutyl phthalate (DBP) through peroxymonosulfate (PMS) activation by cobalt-based

MOF [66]. Co-BTC (A) and Co-BTC (B), were synthesized by two different methods using

trimesic acid (BTC) as a linker. With Co-BTC (A), a higher [DBP] degradation rate was

reached compared to Co-BTC (B) [66]. MOF's recyclability was also established for five

times where no remarkable reduction in the degradation rate of [DBP] [66]. Nevertheless,

as Co is considered as one of the toxic heavy metals, its use may not be favorable to both

human health and the quality of the environmental systems established [10]. For instance,

iron based MIL88-A was used by Yi et al. to activate persulfate successfully decolorizing

Rhodamine B (RB) in water [37]. Results showed that MIL88-A can be used as an efficient

recyclable heterogeneous catalyst for decolorizing RB in water [37].

1.7 Sulfamethoxazole as a Target/model molecule

In this study SMX (Fig.1) was the probe selected for the degradation process. It is an

antimicrobial agent, which is used to treat a variety of bacterial infections such as middle

ear, urine, and respiratory infections. Due to its overuse, its active molecules reach the

surface and ground water due to different industrial and domestic activities. Studies showed

that it is present at low concentrations in surface water around the globe (e.g. 21 ng L^{-1})

[67], nevertheless, this low concentration cause certain modifications in the microbial

community structure leading to antibiotic resistance in environmental microbial

communities [68–70]. This necessities its elimination at its point sources. Traditional waste

water treatment methods have been proven to be insufficient for its the elimination due to

17

its high chemical stability and resistance to biodegradation [3]. Several research groups have investigated the elimination of SMX from waste water by chlorination [71], ozonation [72] photo-Fenton and solar photo-Fenton [73,74], and photo-catalysis [75–77]. All the mentioned treatment methods are energy and catalyst consuming, sometimes leading to stable and toxic metabolites. Accordingly, advanced oxidation processes using PS have been widely investigated due to their advantages in terms of non-toxic byproducts formation (sulfates) and low cost [23]. For instance, SMX removal was demonstrated by Ghauch et al. and Ayoub and Ghauch through PS assisted micrometric Fe^0 as well as bimetallics and trimetallics iron-based particles in aqueous solution [34,78]. Results showed that chemical activation of PS through Fe^0 particles is an effective way for SMX complete degradation in less than two hours [34]. However, all the above mentioned systems lack the option of recyclability and reproducibly rendering the systems to be relatively expensive and can generate some sludge due to iron corrosion products (ICPs) formation. So, in this paper a heterogeneous catalyst (MIL88-A) will be used to activate PS.
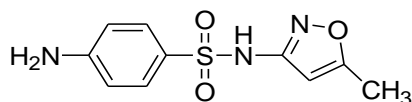
Fig. 1. Chemical structure of Sulfamethoxazole.

1.8 The choice of MILL88-A in the study

First, the choice of MOF in this study was based on several factors. It must contain an activator for PS such as a metal. Iron is considered one of the most suitable metals for PS activation since it is abundant, relatively safe, easy, and affordable to produce. On the other

hand, the choice of ligand, the MOF's second component, is also based on similar criteria

such as affordability, safety, and abundance on which MIL88-A fits both requirements.

MIL88-A is composed of ferric chloride as a metal source and fumaric acid (Fig.2) as a

ligand. The synthesis of MIL88-A is based on water as a solvent in contrary to most other

MOFs that require organic solvents [66,79].

Second, we tried to find a low-cost ligand which is fumaric acid in our case and a

green synthesis method which is based on water as a solvent not an organic one. In fact,

Wang et al. studied the catalytic activity of MIL88-A with PS for the degradation of orange

G (OG), where MIL88-A synthesized at 85ºC for two hours gave the highest degradation

rate of OG that reached 96.4% [42].These results drove our attention of the use of MIL88-

A as PS activator in this study.

$$HOOC \quad H$$
$$C{=}C$$
$$H \quad COOH$$
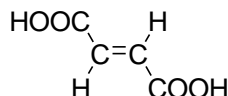
Fig. 2. Chemical structure of fumaric acid

1.9 Structure and porosity of MIL88-A

The three dimensional framework of MIL88-A are built up from oxo-centered trimers

of Fe^{3+} in an octahedral coordination with the ligand: fumaric acid as shown in the

below model (Fig. 3). This framework is formed of trigonal bipyramidal cages of

trimers between which microporous channels are lying along the c-axis. The absence of

any linkages between the trimers within the (ab) plane is at the reason behind the

flexible character of these crystals .
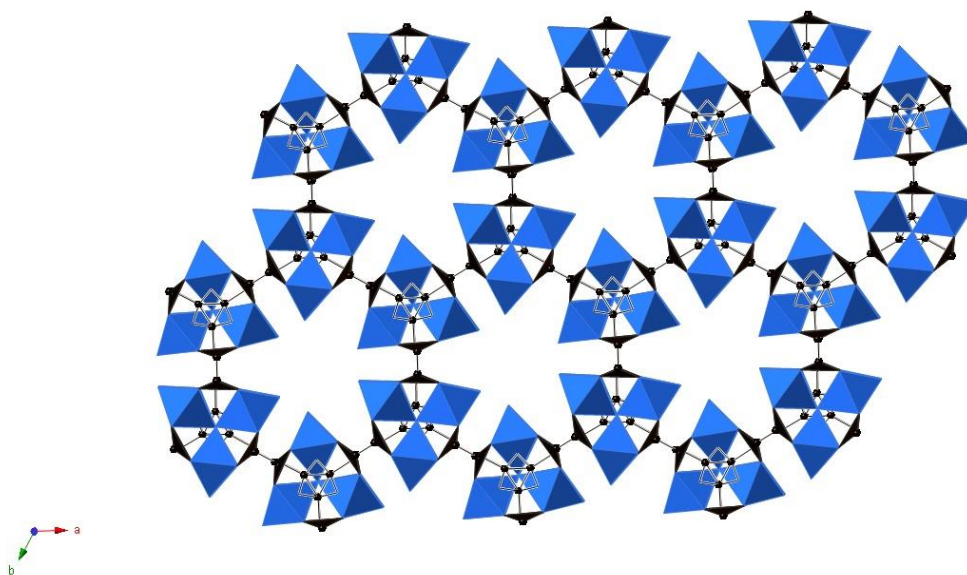
Fig. 3 MIL88-A structure in its open form.

1.10 Objective

We tried in this work to explore additional factors that can improve the properties of

MIL88-A in aqueous solutions and play the role of PS activator in a heterogeneous medium

with the possibility of showing some synergistic effect. For example, we investigated the

combination of PS activators in systems such as UVA/MIL88-A/PS or solar /MIL88-A/PS

and monitored the impact on SMX removal in terms of degradation rate and transformation

products nature and persistence using Time of Flight high resolution mass spectrometry

(ToF HRMS). Moreover, we studied the effect of various factors such as salinity,

carbonates and phosphates on the performance of both systems UVA/MIL88-A/PS/SMX

and solar/MIL88-A/PS/SMX toward PS degradation and the potential application of this

system on real pharmaceutical industry effluents.

CHAPTER 2

MATERIALS AND METHODS

2.1 Chemicals

Sulfamethoxazole (SMX) ($C_{10}H_{11}N_3O_3S$) was obtained from Sigma Aldrich (USA), sodium persulfate (PS) ($Na_2S_2O_8$, purity $\geq$ 99%). Potassium iodide (KI) (puriss, 99.0-100.5%) used for PS quantification and phosphate buffer monobasic (H_2NaO_4P assay $\geq$ 99.0%) and dibasic ($HNaO_4P$ assay: 98-100.5%) used to study the effect of phosphate were purchased from Sigma-Aldrich (China, France, and Germany, respectively). Fumaric acid (C_4H_4O) and iron (III) chloride ($FeCl_3$) (both reagent grade >97%) used in the synthesis of MIL88-A were acquired from Sigma-Aldrich (France and Switzerland respectively). Ethanol (absolute) was purchased from Scharlau (Spain). Formic acid and methanol used as HPLC mobile phase were acquired from Loba Chemie (India) and Honeywell (Germany) respectively. Millipore deionized water (DI) was used in the preparation of all solutions. To evaluate the matrix effect, sodium bicarbonate ($NaHCO_3$) and sodium chloride (NaCl) were acquired from Fluka (Netherlands). Furthermore, hydrochloric acid (HCl) and sodium hydroxide used to modify the pH were purchased from Fluka (Switzerland, Germany, respectively).

2.2 Synthesis of MIL88-A

MILL-88-A was synthesized using the hydrothermal synthesis technique as previously reported by several researchers [37,62,80], this method was selected since it is greener than

the conventional solvothermal method. It was done by adding 1,949 mg of fumaric acid and 4,544 mg of ferric chloride to a beaker containing 84 mL of DI water. The solution was stirred to homogenize for an hour using a magnetic stirrer at 300 rpm. Later, the solution was transferred to a 100 mL Teflon-lined stainless steel autoclave bomb and heated in an oven at 85ºC for 24 hours. The autoclave bomb was then removed and left to cool passively before opening. After which, the solution containing suspended MIL88-A crystals was transferred to two 50 mL Falcon tubes to be centrifuged at 4000 rpm (G-force = 2200) for a period of 10 min. The crystals were then collected, transferred to a 400 mL beaker and then washed three times with 390 mL of ethanol/DI 1:1 solution followed by two consecutive DI washes. This washing process was followed to insure the complete removal of all unreacted fumaric acid and ferric chloride. The precipitate was recovered after each wash by centrifugation using the aforementioned conditions. Finally, the precipitate was dried in a vacuum oven at 100ºC for no less than 10 hours. Each synthesis yielded 2,350 ± 220 mg of MIL-88-A powder which was characterized to insure its purity.

2.3 Characterization of MIL88-A

MIL88-A was characterized according to the common techniques reported in literature [62]. First, to guarantee the crystallinity of the obtained crystals, a D8 Advance (Bruker) X-ray diffractometer (XRD), equipped with copper anode material (40 mA, 40 kV) was used to determine the X-ray diffraction pattern. MIL-88-A was set on a zero-background holder and scanned with a scanning rate of 0.02º per second from 5º to 20º (2Θ). To identify the morphology of the synthesized material a scanning electron microscope (SEM), Tescan, Mira III was used. Also, to determine accurate surface area and pore size of MIL-88-A a

Brunauer-Emmet-Teller (BET) surface area and pore size analyzer (Micromertics, 3 flex surface area characterization) was used Furthermore, a Micromeritics, Q2000 dynamic light scattering instrument (DLS) was used to calculate the hydrodynamic diameter, particle size distribution and zeta potential. In addition to that, MIL-88-A thermogravimetric analysis (TGA) was conducted in a nitrogen atmosphere with a heating frequency of 5° C min^{-1} and a temperature of 30 to 900 °C using a TG 209 F1 Iris (Netzsch, Germany). Finally, a Bruker Tensor 27 IR was used to determine the Fourier Transform Infrared Spectroscopy (FTIR) of the TGA analyzer exhaust under nitrogen. The XPS measurements were performed with a VG ESCALAB 220iXL spectrometer (Thermo Fisher Scientific) utilizing focused mono-chromatized Al Kα radiation (1486.6 eV) of a beam size of ~500 μm^2 (power of 150 W). The measurements were done on the MOF crystals being mixed with 10% conductive carbon (Super-C 65, Timcal). The pressure in the analysis chamber was approximately 2×10^{-9} mbar. The spectrometer was calibrated on the clean silver surface by measuring the $Ag3d_{5/2}$ peak at a binding energy (BE) of 368.25 eV with a full width at half maximum (FWHM) of 0.78 eV. All the spectra were recorded under the conditions of 30 eV pass energy and 50 eV for the surveys in steps of 50 meV and dwell time of 50 ms. The calibration of the binding energy peak positions is applied on the C1s located 284.6 eV [81].

2.4 Experimental conditions and procedures

All solutions were prepared on daily basis using DI water. SMX stock solution (100 ppm) was prepared by dissolving 100 mg of SMX in 1000 mL volumetric flask. The

solution was stirred overnight away from light. PS stock solution (100 mM) was prepared by dissolving 2,381 mg of sodium persulfate in a 100 mL volumetric flask.

For all the experiments that were carried out in the laboratory in the presence of UVA, the required volume of SMX stock solution was added to a 400 mL beaker along with a specific volume of DI. After which, at t_0, the essential amount of MIL88-A was added and left to stir for one minute. The reaction was initiated by the addition of PS solution and turning on the UVA lamps. In order, to ensure consistent mixing and accumulation of MIL88-A, continuous stirring was established throughout the 120 min reaction time. Samples were taken immediately before and after the addition of MIL88-A as well as before and after spiking with persulfate. After which samples were taken every 20 min till t = 120 min. All samples were filtered using 0.45 μm PTFE 13 mm disc filters (Jaytee Biosciences Ltd., UK) and later stored at 4ºC in amber HPLC vials for a maximum period of 12 hours before analysis.

On the other hand, for the experiments that were carried out through this work under solar irradiation, a definite amount of MIL88-A was added to a home built rotisserie shaker that was placed directly under the sun light as shown in the figure below, then a required volume of SMX was added along with a specific volume of DI water. The reaction was initiated by the addition of PS solution, reaction time was set to be 120 minutes whereby samples were taken immediately before and after the addition of MIL88-A as well as before and after spiking with PS. A sample was taken at t = 5 min after which samples were taken every 20 min till t = 120 min. All samples were filtered using 0.45 μm PTFE 13 mm disc

filters (Jaytee Biosciences Ltd., UK) and later stored at 4 ℃ in amber HPLC vials for a maximum period of 12 hours before analysis.

The timing of the sample collection was varied by different experimental criteria.

Control experiments were done either without PS and /or MIL88-A and/or UVA. Experiments were conducted in triplicates and each sample was analyzed twice for uncertainty measurements.

2.5 Reaction setup

Fig. 4. Experimental Setup: six beakers are used as reactors for the performance of SMX removal in UVA/MIL-88-A/PS system where two UVA mosquito lamps are used for irradiating the solution from the top.
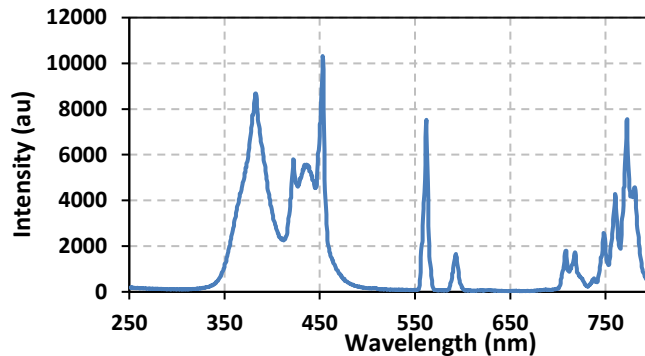
Fig. 5. Emission spectrum of the UVA mosquito lamps used in the experiment.
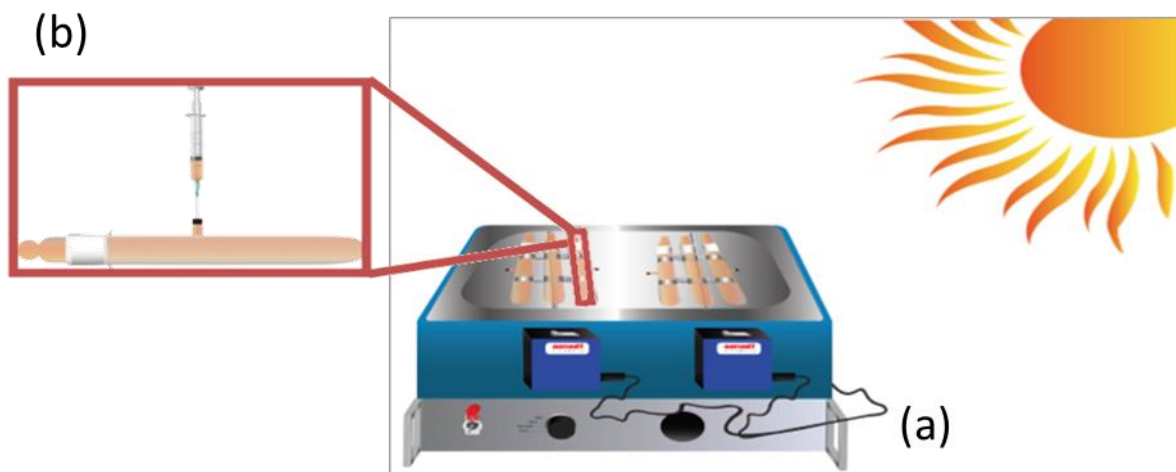
Fig. 6. (a) Reactors used in the solar/MIL88-A/PS/SMX system (b) top view of experimental setup of experiments done under solar irradiation and a single reactor from the rotisserie shaker irradiated system with the syringe showing the sample collecting process.

2.6 Chemical analysis

For the quantification and identification of SMX and its degradation byproducts, a high-performance liquid chromatography device (Agilent 1100 HPLC) equipped with a quaternary pump, a vacuum degasser, an auto sampler with cooling maintained at 4°C, and a thermally controlled column compartment set at 30°C and a DAD detector was used. The

elution process was carried out on a C-18 reverse phase column (5 µm; 4.6 mm internal diameter x 250 mm in length) connected to a security guard column HS C-18 (5 µm; 4.0 mm internal diameter 20 mm long). SMX was quantified at its maximum absorbance wavelength λ = 263 nm. The mobile phase consisted of methanol: 0.1 % formic acid solution of (50:50) (v/v) and was kept under constant flow rate of 0.5 mL min^{-1}. The injection volume was set to 25 µL. Under these conditions, SMX was eluted at a retention time of 6.3 min. The linear dynamic range (LDR) obtained was between 0.1 and 10 mg L^{-1} with limit of detection = 0.0009 mg L^{-1} as it appears in Fig. 7. According to the methods developed by Baalbaki et al [82].
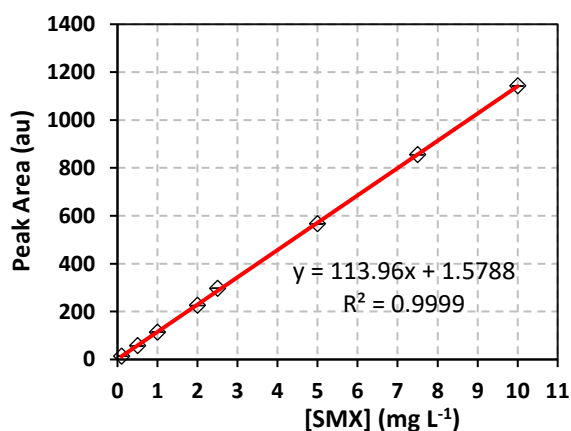
Linest Output SMX			
	y = mx + b		
m	113.9558	1.578785	b
s_m	0.552732	2.713177	s_b
R^2	0.999859	5.258659	s_y

(a)   (b)

Fig. 7. (a) Calibration curve of SMX. The error bars are calculated at 95% confidence level. Absorbance = A (mean) $\pm \frac{ts}{\sqrt{n}}$, where t is the student value (t = 2.447 for 6 degrees of freedom at 95% confidence level) and s the standard deviation of 8 replicates. (b) The LINEST output calculated through Excel provided the slope, y intercept, the regression coefficient and all statistical data including standard deviations on variables.

CHAPTER 3

RESULTS AND DISCUSSION

3.1 Characterization of MIL88-A

3.1.1   XRD pattern of MIL88-A

The XRD pattern of MIL88-A showed well-resolved peaks at 2θ positions of 7.7˚,
10.6˚ and 12.9 ˚ (Fig. 8a). These peaks, although they don't exactly confine with what was
reported experimentally in the literature [62,83]; are consistent with the theoretical
simulated ones, indicating the crystalline nature of MIL88-A.

3.1.2   SEM images of MIL88-A

SEM images showed hexagonal crystals having single phase morphology typical of
MIL88-A, with sizes ranging from 100 to 800 nm (Fig.8 c,d) similar to what was obtained
with other researchers.[62,83]. This was further verified by dynamic light scattering
analysis that revealed an average hydrodynamic diameter of 411 nm with the distribution
profile of the hydrodynamic diameter presented in Fig. 9. In the DI matrix, zeta potential
analysis was carried out as well. The values obtained ranged from -5 mV to + 5 mV,
suggesting that MIL-88-A crystals are vulnerable to settling and require continuous stirring
in order to remain suspended.

3.1.3   BET analysis of MIL88-A

BET analysis showed good adsorption and desorption phenomena as presented in the

isotherms of Fig. 8b. The surface area of MIL88-A was calculated equal to 41.44 m^2/g

which is slightly higher than that reported in literature ranging from 19 to30 m^2/g [62].

3.1.4   TGA and FTIR analysis of MIL88-A

The TGA analysis (Fig. 8e) revealed a 6 % weight loss at furnace temperature below

100 ºC. This is mostly due to water evaporation from MIL88-A sample. Then, a second

weight loss (14.7%) was observed and attributed to the dissociation of the organic linker

(fumaric acid) that is used in the synthesis process of MIL88-A sample, which proceeded

till 400 °C, where a significant weight loss of 30% is detected, after which a complete

breakdown of fumaric acid is observed at around 600 °C resulting in a final weight loss of

14% before ash remains. A different pattern of total dissociation was observed with pure

fumaric acid at around 300 °C and was reported before in literature [84]. It is suggested that

the thermal stability of fumaric acid increases when it is entrapped within MIL88-A

framework, requiring a higher temperature for its dissociation, which was then validated by

the FTIR analysis (Fig. 10). Results showed three significant signals at 3 different

temperatures (316, 445 and 613 °C). In fact, the obtained spectra showed bands

characteristic of the following functional groups: (i) O = C = O stretching at 2350 cm^{-1} at

all temperatures; (ii) C = C = O stretching at 2100–2150 cm^{-1} at temperature 613 °C

confirming the existence of fumaric acid residues at t $\geq$ 300 °C.

3.1.5 XPS analysis of MIL88-A

XPS analysis of MIL88-A was conducted before and after experiment, as it can be noticed from Fig. 11 that the oxidation state of the Fe within the MOF powders on the three prepared samples (as synthesized, after experience without UV, after experience with UV) were examined by XPS, the Fe $2p_{3/2-1/2}$ and O 1s core levels are presented showing the same features confirming that the oxidation state of the Fe remains the same after the experience. The Fe $2p_{3/2}$ and Fe $2p_{1/2}$ binding energy are measured at 712.4 eV and 726 eV respectively. The binding energy position as well as the presence of a satellite peak at 719.4 eV are characteristic of Fe in oxidation state of +3 like in Fe_2O_3.

(a)   (b)
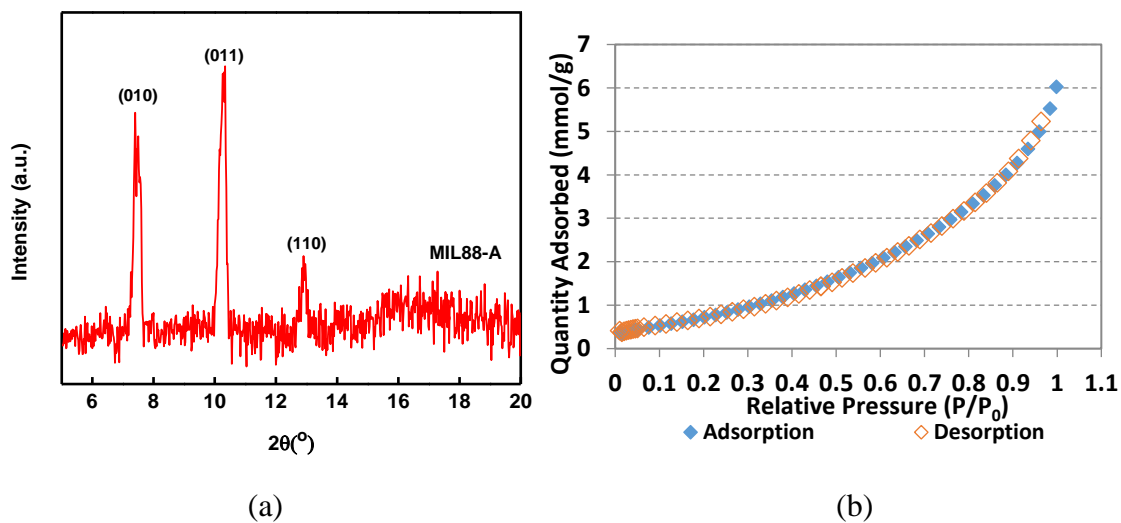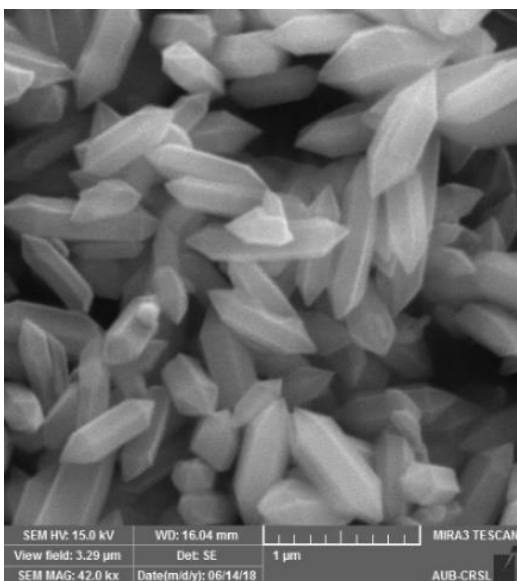
(c)
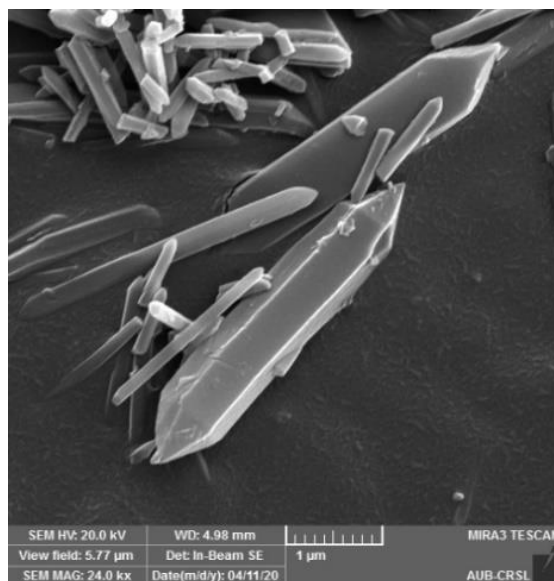
(d)
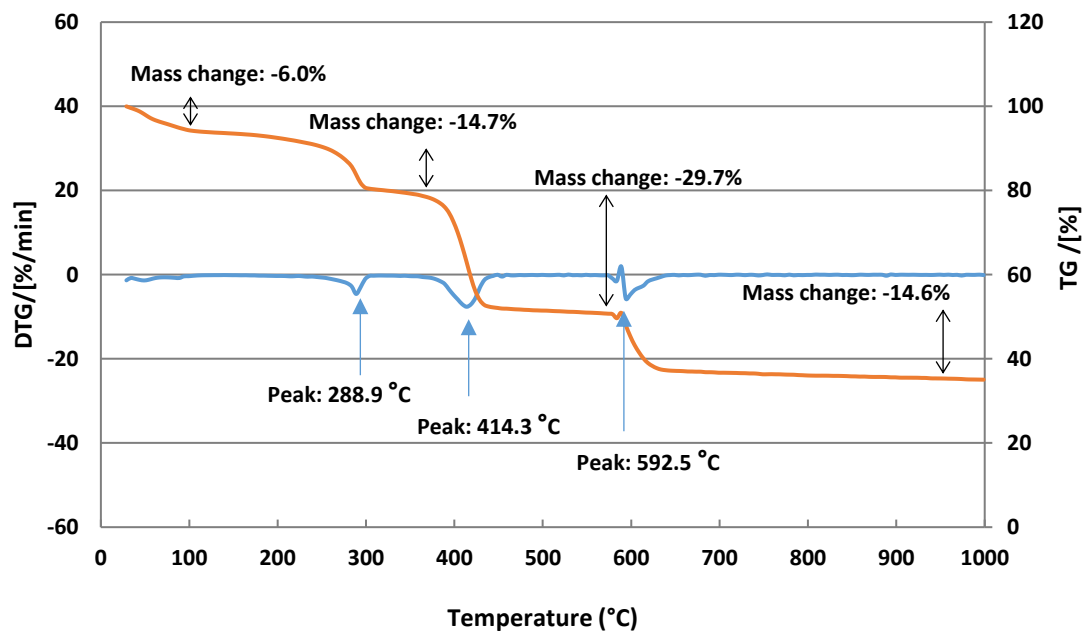
(e)

Fig. 8 Characterization of synthesized MIL-88-A: (a) XRD diffraction pattern SEM of crystals at different magnifications (b) BET adsorption/desorption isotherms [85], (c,d) SEM of crystals at different magnifications and (e) TGA analysis [85].
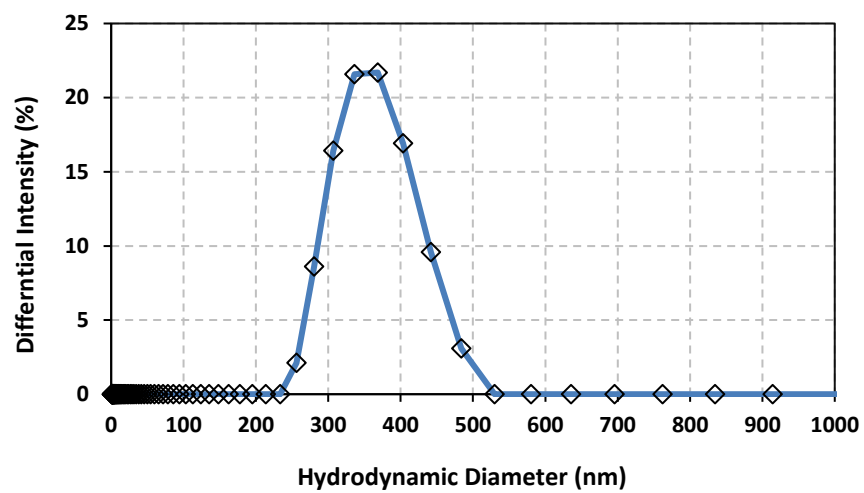
Fig. 9 Hydrodynamic diameter distribution profile of the synthesized MIL-88-A determined using DLS [85].

613 ° C
1 peak at 2350 cm^{-1}
characteristic of
O=C=O stretching.
2 peak at 2100 and
2150 cm^{-1}
characteristic of
C=C=O

326, 444.8 ° C
1 peak at 2350 cm^{-1}
Characteristic of
O=C=O stretching
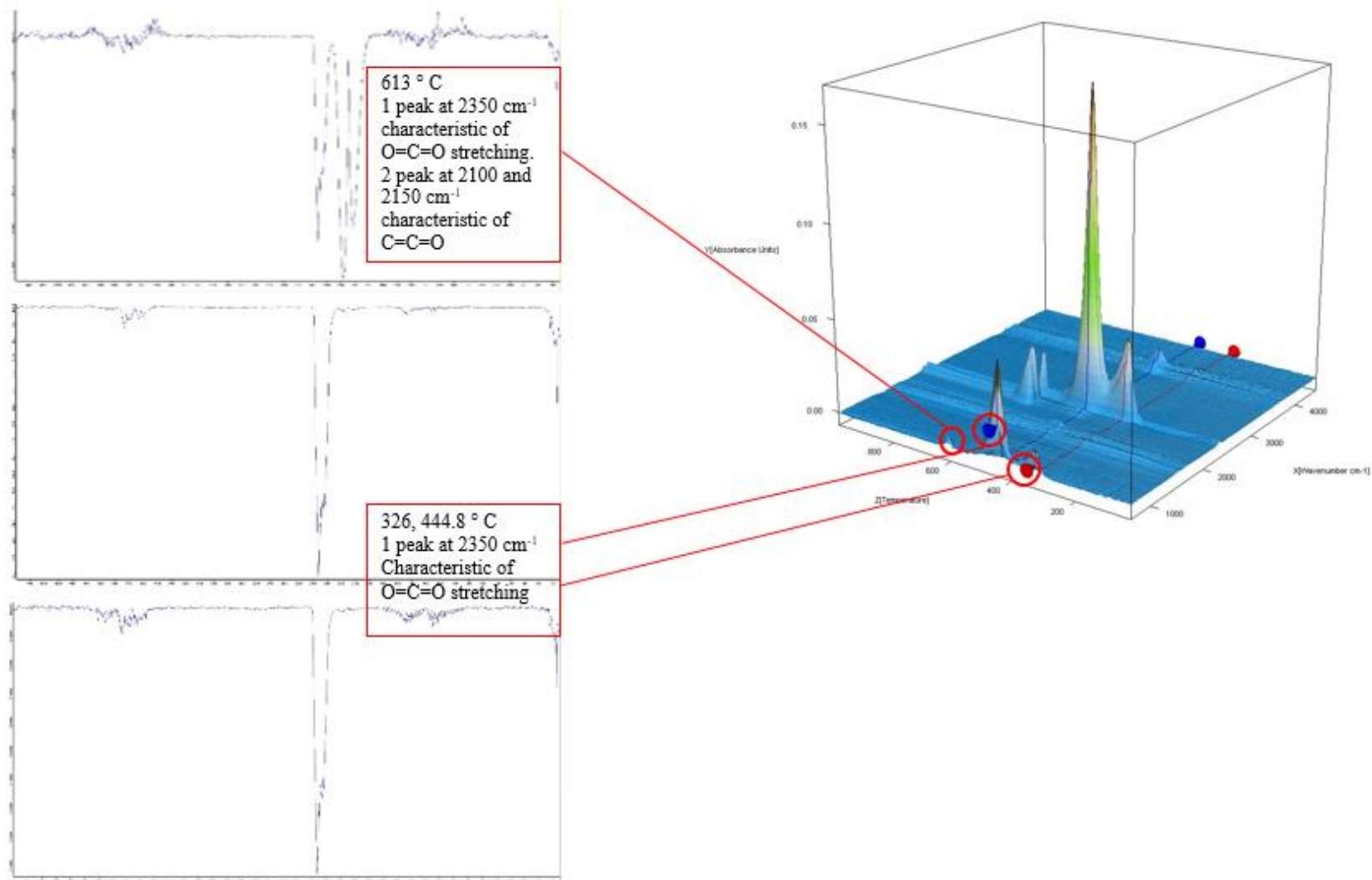
Fig. 10 TGA-FTIR analysis of the synthesized MIL-88 [85].

33

(a)

(b)

(c)

(d)
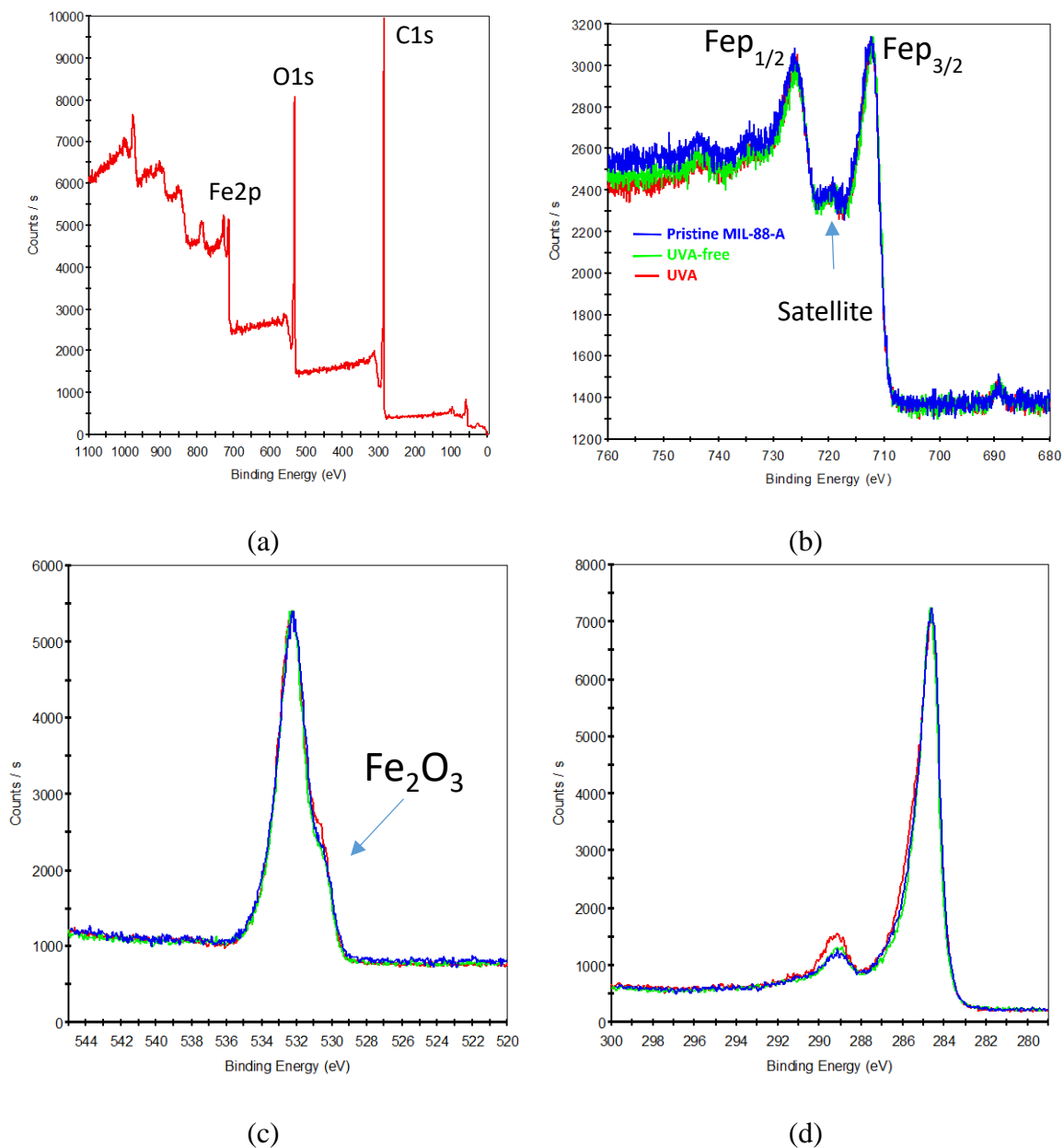
Fig. 11 XPS analysis of pristine MIL-88-A and used MIL-88-A in UVA-free and UVA-irradiated systems after the oxidation reaction. (a) XPS survey spectra, (b) Fe2p$_{3/2-1/2}$ spectra, (c) O1s spectra and (d) C1s spectra. XPS spectra of all samples are almost overlapping everywhere with no significant difference.

3.2 MIL88-A/PS/SMX system in the absence of UV

A preliminary experiment was conducted to test the capability of MIL88-A for
activating PS in the absence of illumination (in dark). 50 mg of MIL88-A was added to a
200 mL solution containing $[SMX]_0 = 10$ ppm and $[PS]_0 = 2$ mM. The reaction time was
set to be 2 hours whereby samples were taken every ten minutes for the first hour followed
by a single sample at t = 120 min. Control experiments were also conducted, in which SMX
degradation was tested in the presence of MIL88-A as well as PS only under the above
mentioned conditions. Both controls showed a sudden drop of a 10% and 12% at t = 0 min
respectively, after which the [SMX] remained constant. This shows that PS only and
MIL88-A only are not effective in the degradation of SMX. For the case where MIL88-A
and PS are combined the % degradation of [SMX] was around 21% after a period of 2
hours. This indicates that MIL88-A/PS system requires assisting agent for the effective
elimination of SMX as shown in Fig. 12.
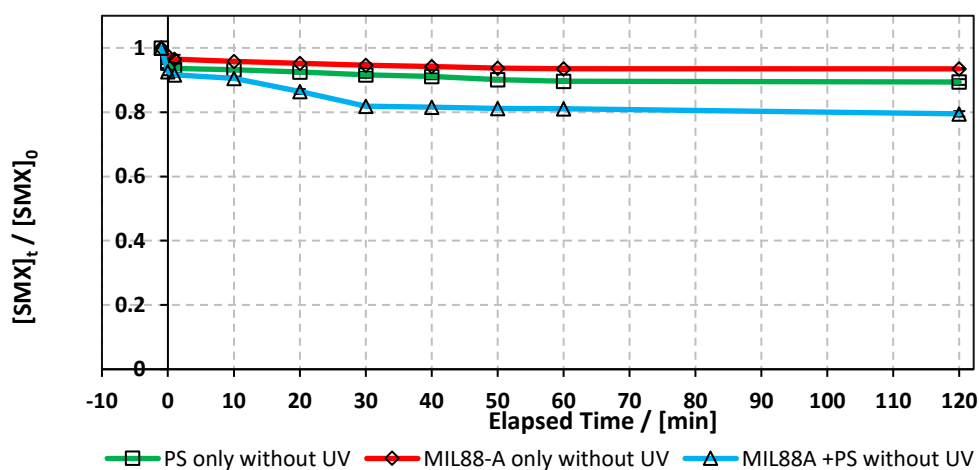
Fig. 12 Elimination of SMX by MIL88-A in the presence and absence of PS as well as with PS
only in beakers on top of a multi-stirrer. Experimental conditions: $[SMX]_0 = 10$ ppm, $[PS]_0 = 2$
mM, $[MIL88\text{-}A]_0 = 250$ mg L^{-1}. Vertical bars represent standard deviations of the means; absent
bars fall within symbols. Sample before t = 0 min was taken before the addition of PS, PS addition
at t_0.

3.3 UVA/MIL88-A/PS/SMX system

In an attempt to improve SMX degradation process in MIL-88-A/PS system, experiments were carried out under UVA irradiation. The latter has been demonstrated by different studies [37,86], an effective factor to enhance the activation of PS initiated by an iron-based system, which is the case here. Reconversion of Fe (III) into Fe (II) species takes place upon UVA irradiation, therefore forming a redox cycle for a sustained PS activation in the reactive medium (Eq. (4)).The UVA/MIL88-A/PS/SMX system was tested against two control experiments: MIL88-A/UVA/SMX and PS/UVA/SMX systems. The % degradation of [SMX] was around 15% with MIL88-A alone after 120 min reaction time, which implies that no significant adsorption of SMX on MIL88-A took place (upper curve). The rate of [SMX] degradation increased to reach around 20% in the UVA/PS/SMX system. This is mostly due to the generated SRs generated upon PS photolysis. However, [SMX] degradation almost tripled when the MIL88-A/PS system was irradiated with UVA to reach 60% after 120 min of experiment time, with MIL88-A playing an additional role as a heterogeneous catalyst in the reaction medium as shown in Fig. 13.
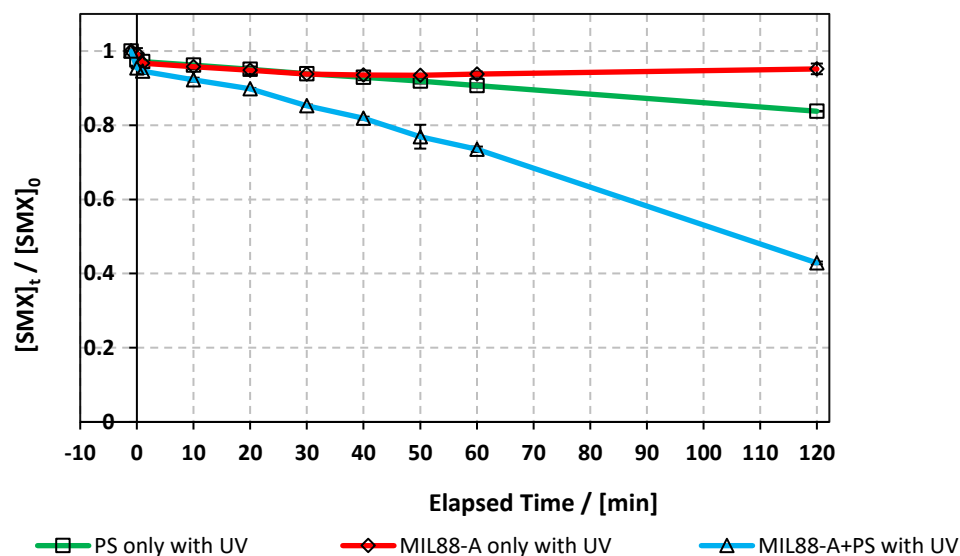
Fig. 13 The % degradation of SMX irradiated with UVA lamps as function of time (min) in three reactions under different conditions: PS only, MIL88-A only, and MIL88-A with PS. Reactors were irradiated by the UVA lamps placed on the side. Experimental conditions: $[SMX]_0 = 10$ ppm, $[PS]_0 = 2$ mM, $[MIL88-A]_0 = 250$ mg L^{-1}. Vertical bars represent standard deviations of the means; absent bars fall within symbols. Sample before t = 0 min was taken before the addition of PS, PS addition at t_0.

3.4 UVA/MIL88-A/PS/SMX system experiments and optimization

3.4.1 Optimization of the UVA irradiation

In this part, the distribution of the UVA irradiation was adjusted. The first experiment was accustomed in a way that the UVA lamps are placed on the side of the reactors. The results obtained showed lower degradation rate (Fig. 12) than when the lamps were placed on the top of the reactors (Fig. 14); in the latter case the reactors were subjected to the highest UVA intensity, thus a higher number of SRs are produced as well as more reconversion of Fe(III) into Fe (II) species is possible.

37
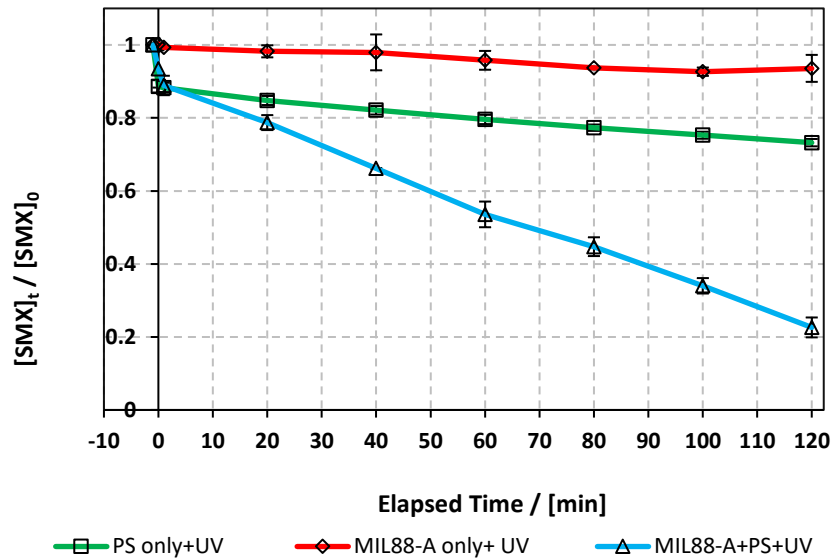
Fig. 14 SMX elimination by MIL88-A/PS/UVA system as function of time (min). Experimental conditions: $[SMX]_0 = 10$ ppm, $[PS]_0 = 2$ mM, , $[MIL88-A] = 250$ mg L^{-1}. Reactors were irradiated by the UV lamps placed on the top. Vertical bars represent standard deviations of the means; absent bars fall within symbols. Sample before $t = 0$ min was taken before the addition of PS, PS addition at t_0.

3.4.2   *Effect of [MIL88-A]$_0$*

Three different concentrations of $[MIL88-A]_0$ 10 mg/L,125 mg/L and 250 mg/L were tested at fixed $[PS]_0$ (2 mM). This was demonstrated so that we can identify the minimum amount of the catalyst that should be added to the reactive medium to achieve complete degradation of SMX is within 5 hours. Results showed that all the tested concentration of MIL88-A was accompanied by 100% degradation of SMX but at different reaction rates. It

was witnessed that 125 mg/L of MIL88-A showed the highest rate, so this concentration

will be adopted to carry out the rest of the experiments as shown in Fig. 15.
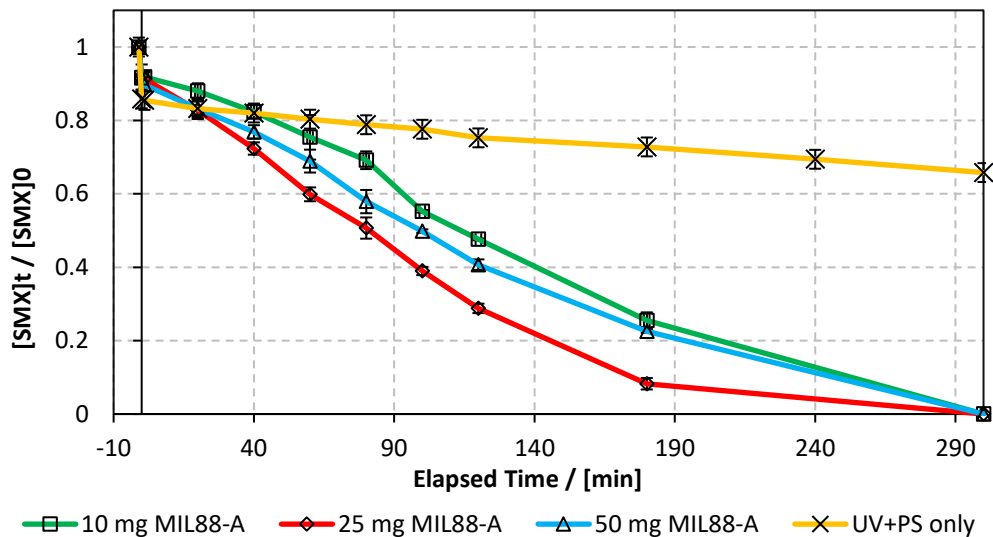
Fig. 15 The % degradation of SMX as function of time (min) using three different masses of MIL88-A (50 mg, 25 mg and 10 mg) are plotted against the control experiment (UVA/PS/SMX system). Experimental conditions: $[SMX]_0 = 10$ ppm, $[PS]_0 = 2$ mM, Vertical bars represent standard deviations of the means; absent bars fall within symbols. Sample before $t = 0$ min was taken before the addition of PS, PS addition at t_0.

3.4.3   *Recyclability*

Throughout the scope of catalytic materials such as MIL-88A, recyclability is an

important variable for assessing its cost / commercial value since a heterogeneous catalyst

can be recovered and used again. In this part, MIL88-A was recovered three times

successively after each experiment. The recovery cycle included the collection of MIL88-A

used then its separation using centrifugation followed by drying in the vacuum oven at

90°C for 24 hours. After that, MIL88-A was used in a second experiment, each time the

quantity of MIL88-A recovered decrease due to the difficulty in collecting MIL88-A since

some of MIL88-A crystals are stuck in the 0.45 um PTFE filter used in the sampling

process. Results showed that 100 % degradation of [SMX] was obtained in the three

successive cycles, however the catalytic activity of MIL88-A improved after each cycle (Fig. 11). For every next cycle the volume of SMX solution (5 ppm) was adjusted in a way to keep the concentration of MIL88-A constant equal to 125 mg/L, in order to do an accurate comparative study of the results obtained from each cycle. The results obtained may be explained first, by the fact that the more the defects in a heterogeneous catalyst the better its catalytic activity and that was clearly inferred from the data shown in Fig. 16 where the first cycle showed around 58% degradation within the first 20 min reaction time compared to cycle 2 and cycle 3 where it reached 65% and 68% respectively. Second, these results demonstrated the high potential of PS in reactivating MIL88-A surface. In order to confirm this hypothesis, SEM images were taken after each cycle, MIL88-A showed rod-like morphology similar to that obtained with freshly synthesized MIL88-A, however MIL88-A crystals lost some of its homogeneity were the crystals were elongated. The XRD pattern of MIL88-A conducted after experiment showed peaks at two theta positions that complies with the freshly prepared MIL88-A.
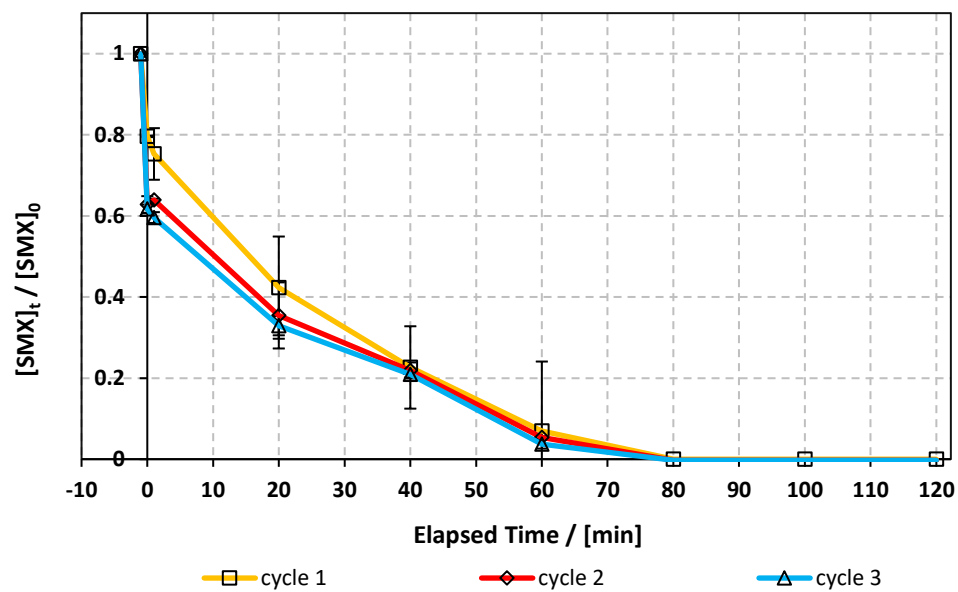
Fig. 16 Recyclability experiments of MIL88-A in the UVA reactors. $[SMX]_0 = 5$ mg L^{-1}. $[PS]_0$ = 2 mM, [MIL88-A] = 125 mg L^{-1}. Error bars are calculated as $\frac{ts}{\sqrt{n}}$, where absent bars fall within the symbols.

(a)   (b)
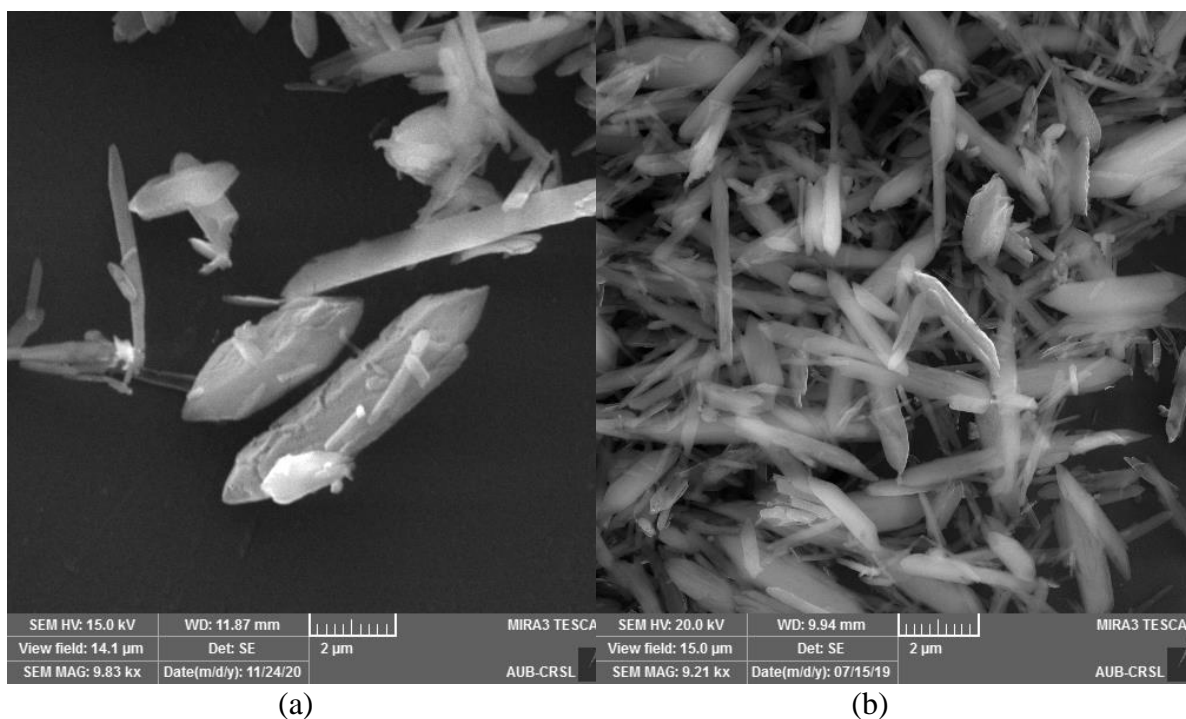
Fig. 17. SEM images of recycled MIL88-A
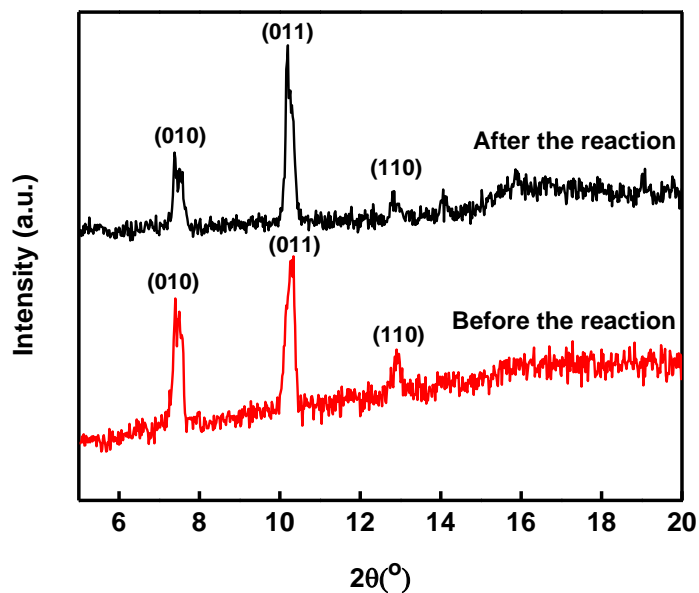
Fig. 18. XRD pattern of newly synthesized and recycled MIL88-A

3.5 Solar/MIL88-A/PS/SMX system

As it can be noticed from Fig. 19, different controls were done to assist the effectiveness of solar/ MIL88-A/PS/SMX system. We witnessed that solar energy kept the medium unchanged whereby the degradation of SMX reached 10% only after 2h. It was clear that solar energy needs an assisting agent to degrade SMX, so PS and MIL88-A were added separately to the system and showed similar trend in the variation of the elimination of SMX reaching 82% and 78 % after 120 min reaction time. This was also suggested by similar AOPs using PS as an oxidant for the degradation of SMX by Ghauch et.al [34] whereby the rate of SMX degradation reached around 20 % in the presence of PS only; this verifies the imperative role of solar power in the generation of more SRs in the system. It is important to mention that the solar flux reached a maximum of 3900 uW/cm^2 initially and

42

decreased to reach a minimum of 1600 uW/cm^2 at the end of the reaction as the reaction started at 11:00 am and ended by 1.00 pm. For instance, throughout the day, the sun rays intensity increases gradually to reach its maximum at noon (12: pm), then decreases at dawn and dusk, and in between at other hours of the day. Other parameters such as cloud cover being equal, a solar panel's output is highest at noon because the sun's rays are more direct than at other times. For example , several studies have also investigated the use of solar power with H_2O_2 as an oxidant in catalysis and showed promising results of TOC removal in waste water treatment [87]. All these control experiments proved that Solar/MIL88-A/PS/SMX is the most effective system in the degradation of SMX reaching 100% after 5 min of reaction time only.
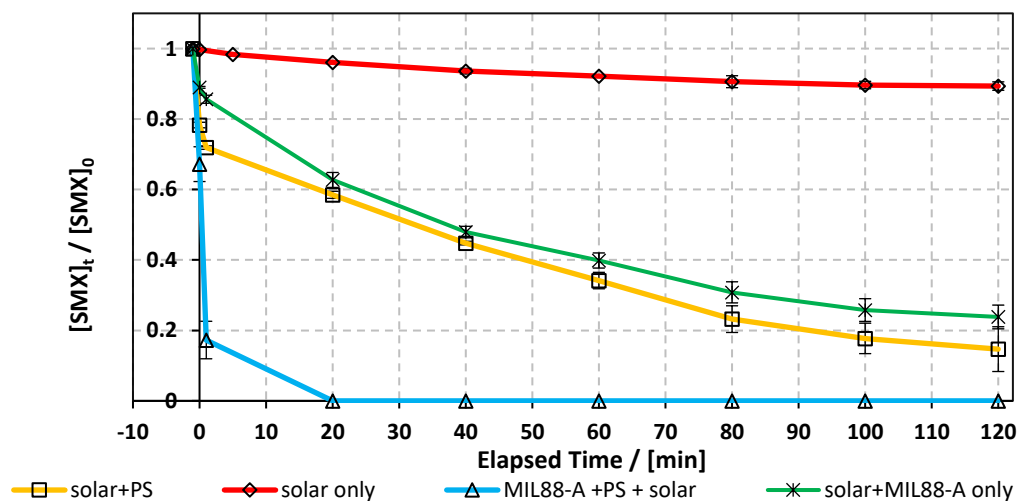
Fig. 19. The % degradation of SMX irradiated with solar energy as function of time (min) under different conditions: PS only, MIL88-A only, and MIL88-A with PS. Reactors were put under sunlight in a rotisserie shaker Experimental conditions: $[SMX]_0 = 5$mg L^{-1}, $[PS]_0 = 2$ mM, $[MIL88-A]_0 = 125$ mg L^{-1}. Vertical bars represent standard deviations of the means; absent bars fall within symbols. Sample before t = 0 min was taken before the addition of PS, PS addition at t_0.

3.6 Matrix effect

3.6.1   Case of chlorides

The influence of common anions in natural water were conducted on SMX degradation in both UVA/MIL88-A/PS/SMX and solar/MIL88-A/PS/SMX systems. Three different concentrations of chlorides corresponding to fresh water ([NaCl] = 200 mg L^{-1}), brackish water ([NaCl] = 2,000 mg L^{-1}), and saline water ([NaCl] = 20,000 mg L^{-1}) were tested to mimic natural water conditions [88]. It was witnessed that in/UVA/MIL88-A/PS system, both fresh water and brackish water show similar trend of the variation in the % degradation of SMX with slight enhancement of the process whereby SMX degradation reached 100% after 80 min similar to that obtained with [NaCl] free experiment. This is mainly due to the formation of chlorine radicals (Cl$^\bullet$) which has a redox potential close to that of SRs (E^0 = 2.4 V) in addition to the formation of reactive hydroxyl radical (HO$^\bullet$) as shown in the below equations. However, SMX degradation was accompanied by a slight inhibition in saline water whereby it reached around 90% after 2h (Fig. 20a). This was not the case in MIL88-A/PS/solar system were the three different concentrations of NaCl had no significant effect on the degradation of SMX (Fig. 20b). These results are in accordance with previous research done on UV/PS activated systems demonstrated by Ghauch et al. [30,32]. In these systems the degradation of ketoprofen was inhibited in brackish and more significantly in saline water where the concentration of Cl$^-$ ions is above 10 mM (584 mg L^{-1} of NaCl) and chloride quenching effect is more evident in the media.

$$SO_4^{-\bullet} + Cl^- \rightarrow Cl^\bullet + SO_4^{2-} \hspace{4cm} (6)$$

$$Cl^• + Cl^- \rightarrow Cl_2^{•-} + SO_4^{2-} \tag{7}$$

$$Cl_2^{•-} + Cl_2^{•-} \rightarrow 2\ Cl^- + Cl_2 \tag{8}$$
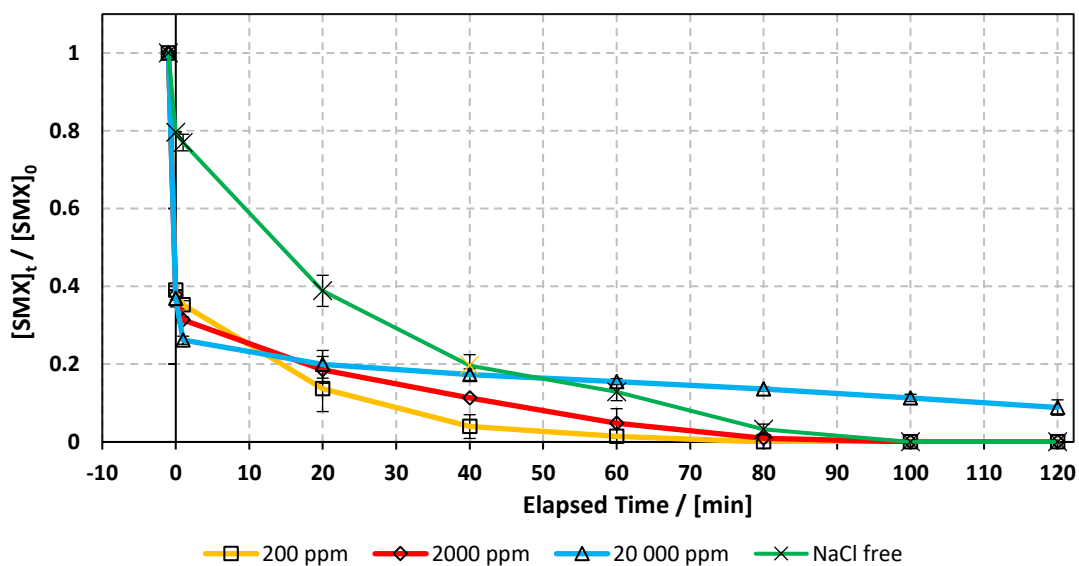
(a)
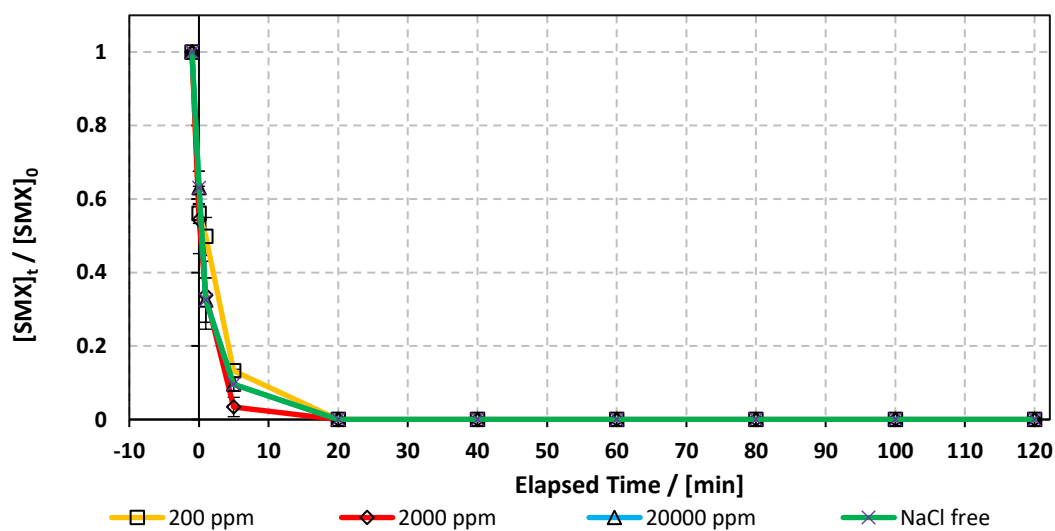
(b)

Fig. 20 Effect of [NaCl] = 200 - 20,000 mg L^{-1} on the degradation of SMX as function of time (min): (a) in the UVA/ MIL88-A/PS/SMX system and (b) in the solar/MIL88-A/PS/SMX system. Experimental conditions [SMX]$_0$= 5 ppm [PS]$_0$ = 2mM, [MIL-88-A]$_0$= 125 mg L^{-1}. Error bars are calculated as $\frac{ts}{\sqrt{n}}$ where absent bars fall within the symbols.

3.6.2   Case of carbonates

The effect of bicarbonate was also demonstrated on both systems UVA/MIL88-A/PS/SMX and solar/MIL88-A/PS/SMX. It is evident that in the first system, the addition of NaHCO$_3$ inhibited greatly the degradation process. In fact, the drop of [SMX] within the first 20 min, with the three tested bicarbonate concentrations (1,50, and 100 mM) decreased from 80.4% to 11.7% keeping around 90 % of SMX in the reactive medium and that after 120 min compared to the NaHCO$_3$ free system where complete degradation was achieved within 80 min (Fig. 21a). However, in the solar/MIL88-A/PS/SMX system, the SMX degradation rate decreased gradually when bicarbonate ions were added to the system regardless its concentration, but a complete degradation of SMX was reached as shown in Fig. 21b. This inhibitory effect of NaHCO$_3$ can be explained by the reaction of SRs with HCO_3^- yielding $CO_3^{\bullet-}$ which have moderate oxidative properties (E° = 1.59 V) compared to that of SRs toward SMX (Eq.6). It is important to mention that the pH of the reactive medium increased from 3.53 to 8.66 in the reactor of 100 mM NaHCO$_3$ which played a major role in ceasing the degradation process.

$$SO_4^{-\bullet} + HCO_3^- \rightarrow SO_4^{2-} + CO_3^{-\bullet} + H^+ \tag{9}$$

Table 1. (a) pH values of the different reaction system during the experiment in the UVA/MIL88-A/PS/SMX system and (b) pH values of the different reaction system during the experiment in the Solar/MIL88-A/PS/SMX system

	pH initial	pH final
[HCO$_3^-$] free	5.63	3.29
[HCO$_3^-$] = 1 mM	6.46	5.31
[HCO$_3^-$] = 50 mM	8.57	8.87
[HCO$_3^-$] = 100 mM	8.66	8.86
(a)		

	pH initial	pH final
$[HCO_3^-]$ free	3.52	3.15
$[HCO_3^-]$ = 1 mM	6.18	3.61
$[HCO_3^-]$ = 50 mM	8.31	8.37
$[HCO_3^-]$ = 100 mM	8.40	8.42
(b)		

(a)

47
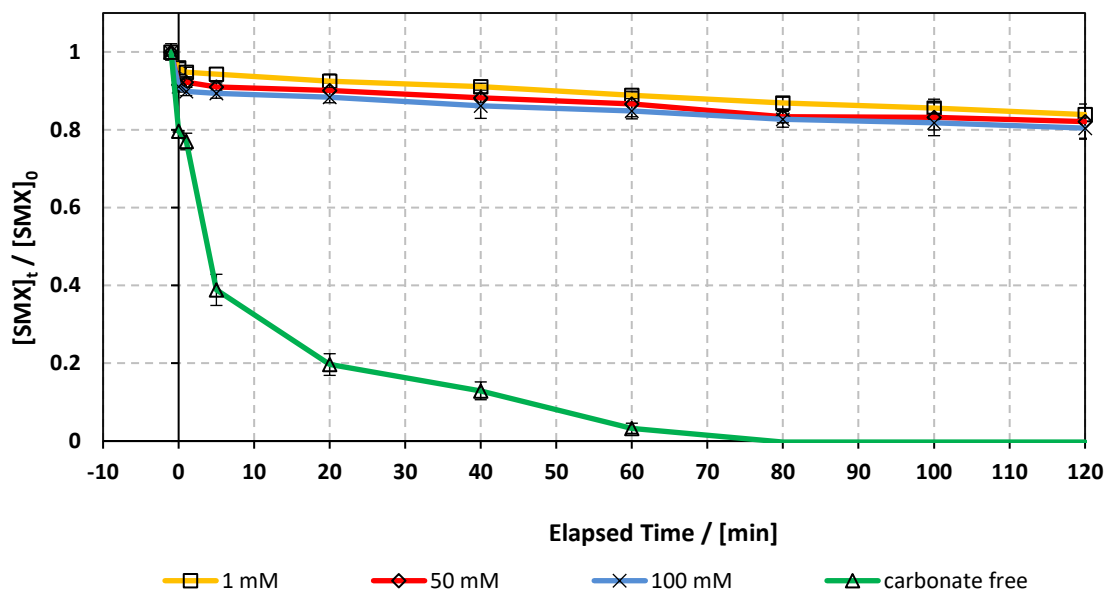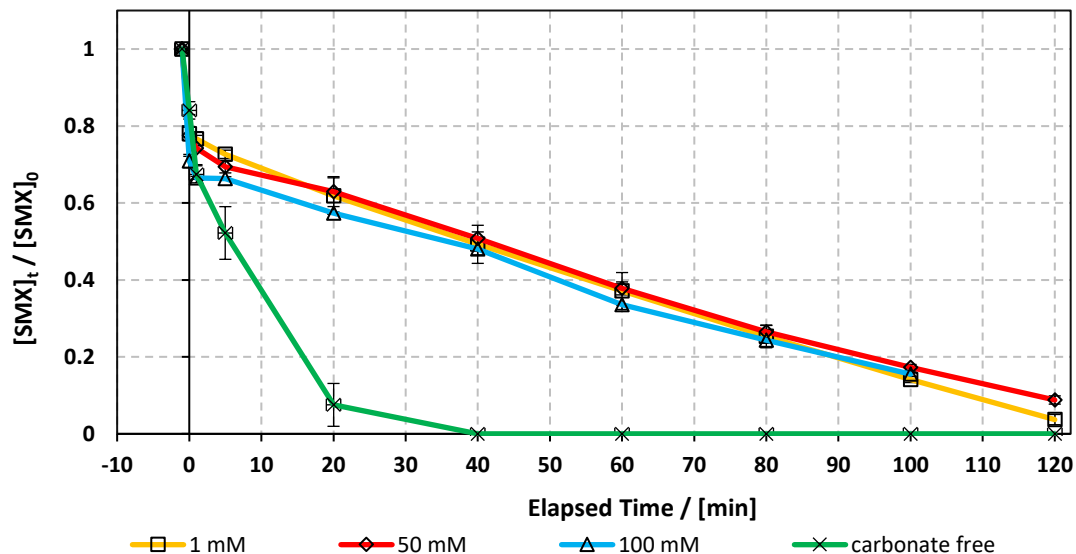
(b)

Fig. 21 Effect of different carbonate concentration $[CO_3^{2-}] = 1 - 100$ mM on the degradation of SMX as function of time (min): (a) in the UVA/ MIL88-A/PS/SMX system and (b) in the solar/MIL88-A/PS/SMX system. Experimental conditions $[SMX]_0 = 5$ ppm $[PS]_0 = 2$mM, [MIL-88-A]$_0$= 125 mg L^{-1}. Error bars are calculated as $\frac{ts}{\sqrt{n}}$ where absent bars fall within the symbols

3.6.3   Case of phosphate

The effect of phosphate on the degradation of SMX was demonstrated for two main reasons. First of all, to account for phosphate residues that may escape from conventional wastewater treatment methods, second to study the pH effect on the degradation of SMX. As we notice from Fig. 22a, the kinetics of the reaction changed after the addition of phosphate buffer (PB) to the system which leads to an instant drop in SMX degradation by 70 % upon addition of PS after which it remained constant through the 120 min reaction time. This was not the case in the solar/MIL88-A/PS system where the degradation rate of SMX reached around 80 % at the end of the reaction with the different concentrations of PB (5, 10 and 20 mM) (Fig. 22b). We can assume that PB has an inhibitory effect on the degradation process of SMX, but it varied differently with the two studied systems. This

48

can be attributed to the fact that phosphate species form stable complexes with Fe^{2+} ions and accumulate on the surface of MIL88-A, thus preventing the chemical activation of PS that is accomplished by free Fe^{2+} ions in solution or adsorbed on the surface of the MOF. This hypothesis was also verified in two independent studies on SMX and ranitidine removal in Fe/PS systems [34,35].

(a)

(b)

Fig. 22 Effect of different carbonate concentration $[PO_4^{3-}]$= 5 - 20 mM on the degradation of SMX as function of time (min): (a) in the UVA/ MIL88-A/PS/SMX system and (b) in the solar/MIL88-A/PS/SMX system. Experim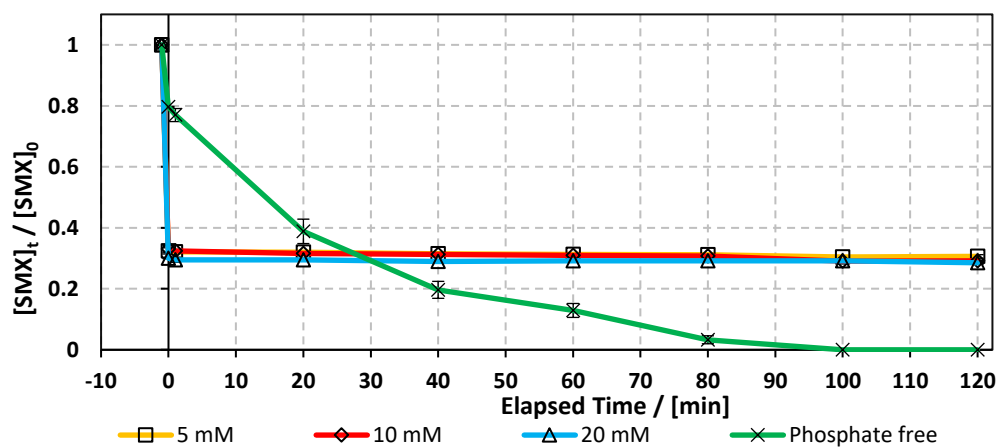ental conditions $[SMX]_0$= 5 ppm $[PS]_0$ = 2mM, [MIL-88-A]$_0$= 125 mg L^{-1}. Error bars are calculated as $\frac{ts}{\sqrt{n}}$ where absent bars fall within the symbols.

3.6.4   *EPR measurements*
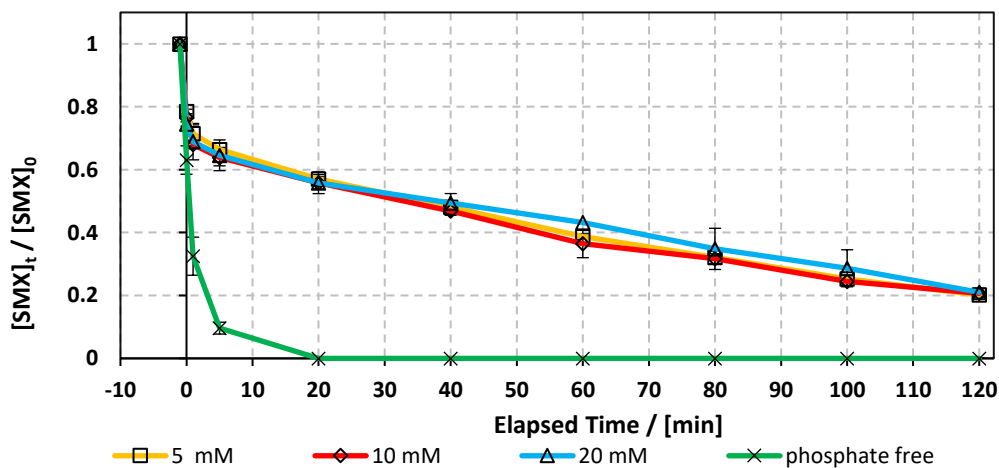
Since we are using MIL88-A as a heterogeneous catalyst to activate PS for the degradation of SMX, it is suggested that SRs and HRs are generated to react with the target molecule (SMX) in an oxidative mechanism to fully degrade it and transform it to harmless species. In such a heterogeneous system, it was challenging to identify the presence of these species with the techniques that were used before with homogenous catalysts such as Fe^{2+} ions in PS- based AOPs [30,89]. In fact, identification of radicals relies on the use of quenchers such as MeOH and TBA however those may highly interfere with MIL88-A active sites. Thus, EPR technique was selected as a proper analytical method to hunt for the presence of these radicals in the system, this was accomplished by the use of 5,5-dimethyl-L-pyrroline N-oxide (DMPO) as a free radical targeting molecule [90–92].

The EPR analysis in this study was done on four different systems: System 1 (MIL88-A), System 2 (PS), System 3 (MIL88-A/PS) and System 4 (MIL88-A/PS/SMX) in order to conduct a reliable comparative study. As it can be noticed from Fig. 24 there are no detectable signals in System 1 compared to the peaks that are shown in the three studied systems (2-4). To better understand the results of the EPR spectra obtained, a simulation on the EPR spectra was conducted via the Easyspin library for MATLAB, whereby the rotational tumbling (5×10^{-11} s) and the 'chili' functions were used [93]. The results showed the presence of DMPO-OH adducts of intensity 1:2:2:1 and a hyperfine splitting constant of $a_N = a_H = 1.49$ mT and another series of six peaks with intensities 1:1:1:1:1:1 that account for DMPO-CH$_3$ adduct and a hyperfine splitting constant $a_N = 1.58$ mT and $a_H = 2.58$ mT (Fig.23). The obtained alkyl radical may be generated from the alkyl leaching from the

organic linker used in the synthesis process of MIL88-A (e.g. fumaric acid) or from ethanol solvent which is used in the washing process. For system 1, one can estimate that the OH radicals present may be generated from the photo activation of MIL88-A under the day light as previously investigated. Moreover, the EPR spectrum of DMPO solution in system 2 shows four peaks attributed to the DMPO-OH adduct with an intensity of 1:2:2:1and a hyperfine splitting constant of $a_N = a_H = 14.9G$ that are much resolved than the ones obtained in system 1 that accounts for the pure formation of HRs. It is important to mention that with time as the measurements are taking place, activation of PS is possible at room temperature, thus unstable, very short lifetime DMPO-SO_4^- adducts are formed. Accordingly, following a rational expectation the production of DMPO-OH adducts are favored in aqueous medium. This could happen either by nucleophilic substitution of DMPO-SO_4^- (Eq. (7)) or by the trapping of OH$^•$ formed (Eq.(8)) as already investigated [94]. Upon spiking with PS (System 4), one can notice, in addition to the DMPO-OH four split lines, six peaks with an intensity of 1:1:1:1:1:1 corresponding to the DMPO-SO$_4^-$ adduct with hyperfine splitting constants of $a_N = 13.9G$, $a_H = 10G$, $a_H = 1.48F$, $a_H = 0.78G$. It is worth noting to mention that measurements done on the same system in the presence of SMX (System 3), showed the presence of the same DMPO adducts however with less improved DMPO-SO$_4^-$ adduct. This can be attributed to the fact that some of the catalytically generated radicals reacted with SMX probe rather than with DMPO resulting in lesser trapping probability. Accordingly, the use of EPR technique helped in identifying the presence of HRs and SRs and their coexistence in solution. Recall that some of the SRs are being converted into HRs upon reaction with water as previously demonstrated. This is

the reason why the intensity of the DMPO-OH adduct are always showing greater amplitude than that of DMPO-SO$_4^-$ adducts in aqueous systems. In conclusion, one can conclude that the degradation process of SMX takes place through radical mechanism since we are able to see both SRs and HRs through the EPR measurements that were demonstrated.

$$SO_4^{-\bullet} + H_2O \rightarrow OH^{\bullet} + H^+ + SO_4^{2-} \tag{10}$$

$$DMPO - SO_4^- + H_2O \rightarrow DMPO - OH + H^+ + SO_4^{2-} \tag{11}$$
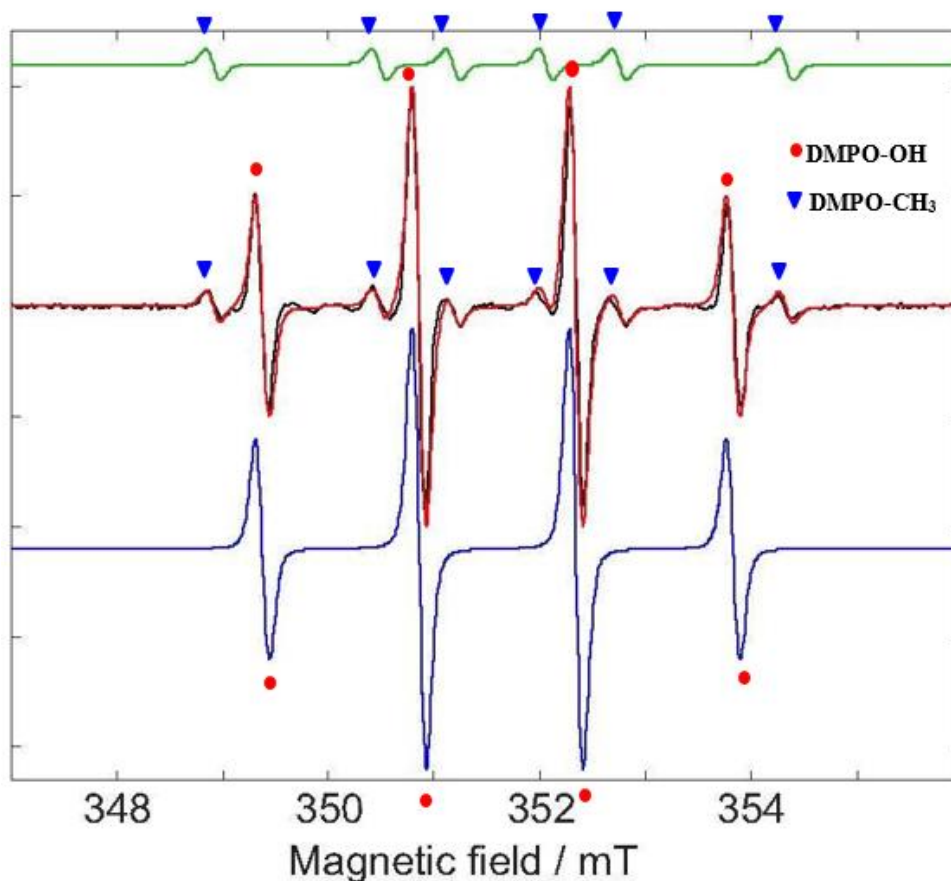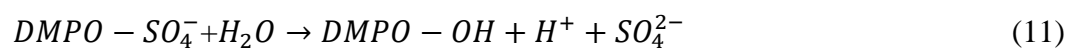
Fig. 23 EPR spectra. Green – simulated EPR spectrum for trapped methyl radicals. a_N =1.58 mT, a_H =2.28 mT. Blue – simulated EPR spectrum for trapped hydroxyl radicals. a_N = 1.49 mT, a_H = 1.49 mT. Red – the sum of the above two simulated trapped radical spectra. Black – experimental EPR spectrum under the following Experimental conditions: [PS] = 2.5 mM, [MIL-88-A] = 12.5 mg L^{-1}, [DMPO] = 100 mM.
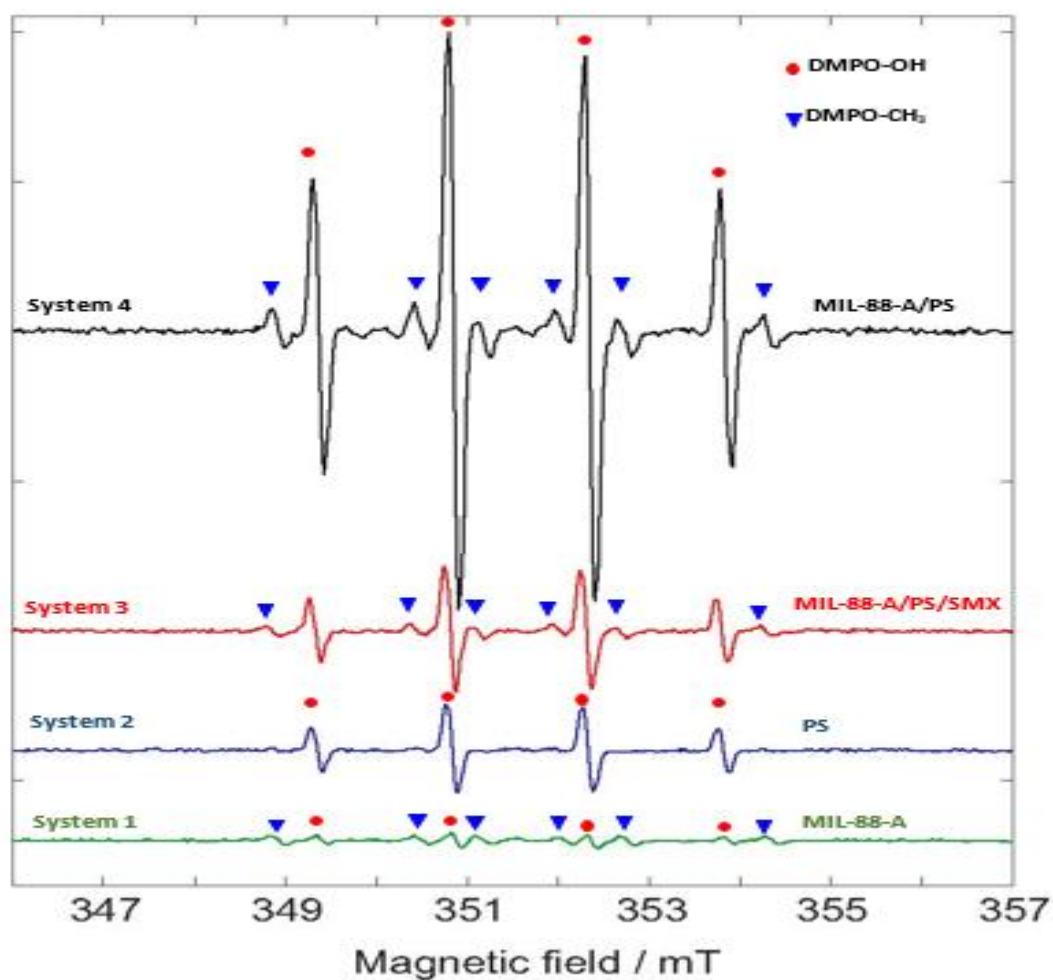
Fig. 24 . EPR spectra of DMPO-radical adducts in different reaction systems. Experimental conditions: [PS] = 2.5 mM, [MIL-88-A] = 12.5 mg L^{-1}, [DMPO] = 100 mM. The acquisition duration of EPR spectra is about 100 min for all systems.

53

3.6.5 Degradation mechanism

a. <u>Identification of degradation products</u>

Under the current experimental conditions, SMX showed through its degradation in MOF-activated PS system the presence of three byproducts as it can be shown in Fig. 25. The identity of these byproducts is further investigated in section 5.3 using high-resolution mass spectrometry.
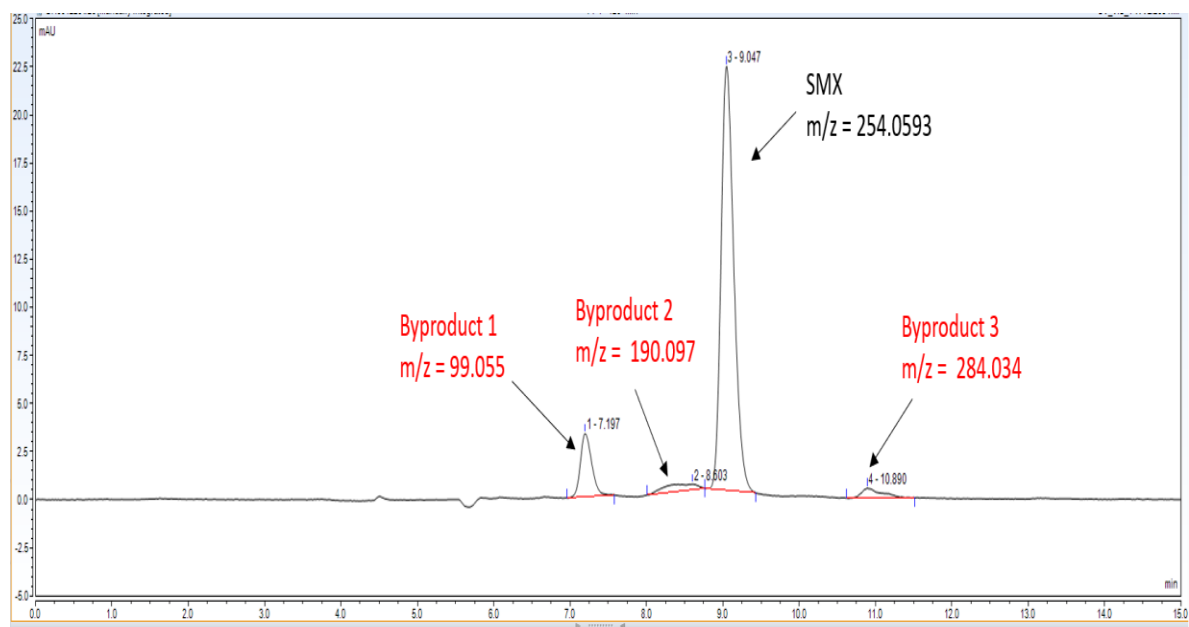
Fig. 25. HPLC chromatogram at T = 25 °C showing SMX and its byproducts at reaction time t= 40 mins.
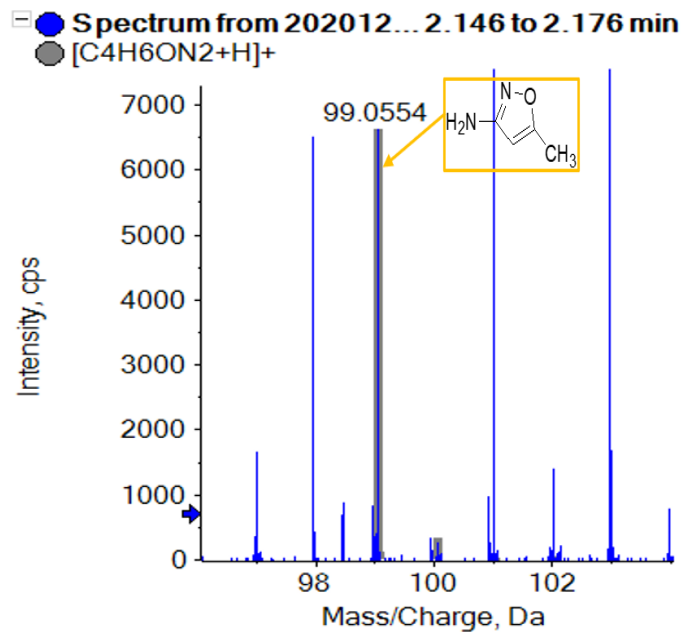
Fig. 26. Mass spectrum fragmentation pattern under oxygen conditions of BP1.
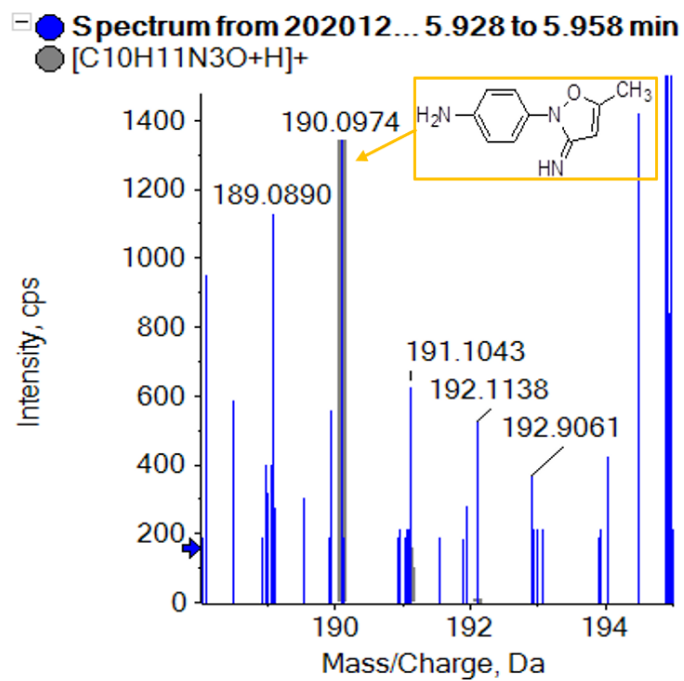
Fig. 27. Mass spectrum fragmentation pattern under oxygen conditions of BP2.
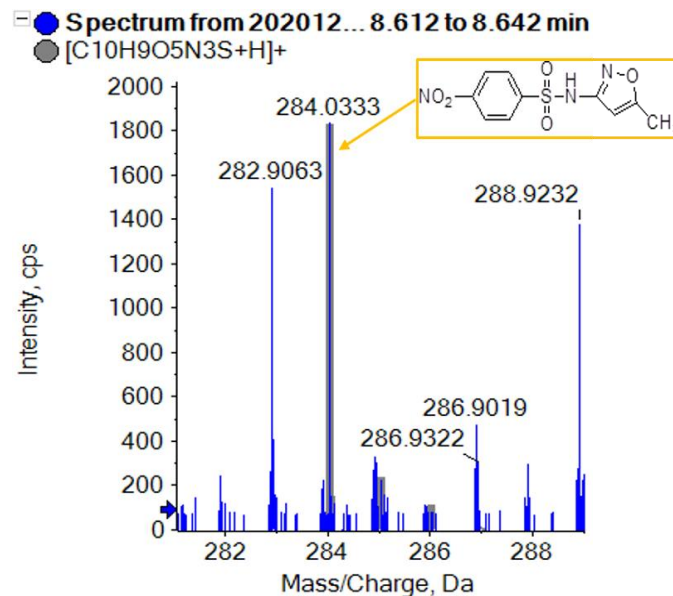
Fig. 28. Mass spectrum fragmentation pattern under oxygen conditions of BP3.

    b. <u>Proposed mechanism Surface based activation of PS on MIL-88A</u>

Based on the EPR measurements, the elimination of SMX in UVA/MIL88-A/PS system

was mainly due to a radical process. For instance, Fe active species present in the MIL88-A

are trivalent since they originate from the ferric chloride salt used in the synthesis process

of MIL88-A through which PS chemical activation may occur by one-electron reduction

mechanism (Eqs. (12) and(13)) as it was previously proven [37,85,95]

$$\equiv Fe^{3+} + S_2O_8^{2-} \rightarrow Fe^{2+} + S_2O_8^{-\bullet} \tag{12}$$

$$\equiv Fe^{2+} + S_2O_8^{2-} \rightarrow Fe^{3+} + SO_4^{-\bullet} + SO_4^{2-} \tag{13}$$

For instance, XPS analysis was demonstrated on three different samples: pristine MIL88-A,

after experiment in the absence of UVA and after experiment in the presence of UVA. As it

can be inferred from Fig. 11, the Fe2p$_{3/2-1/2}$ and O1s core levels of the three tested samples

showed the same structures approving that Fe oxidation state remains the same after the

56
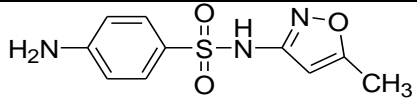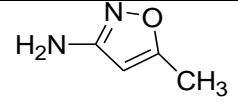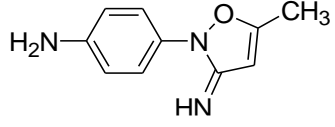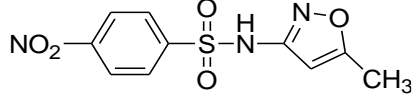
reaction. Results showed binding energy values at 712.4 eV and 726 eV for Fe2p$_{3/2-1/2}$ and O1s respectively. A satellite peak at 719.4 eV was observed also, the presence of this peak and the position of the binding energy are considered as characteristics of Fe in + III oxidation state, which is the case in Fe_2O_3 [96,97]. It is important to mention that Fe in + II oxidation state could be present however it is quickly oxidized to Fe^{3+} in the presence of air or oxygen. Moreover, the hydrolysis of PS and SRs may occur in the reactive medium in the presence of water to generate $SO_4^{-\bullet}$, $O_2^{-\bullet}$ and $OH^\bullet$ in the absence of UVA (Eqs. (14-16)), Fe^{2+} is formed as stated in eq.1, generate unstable PS radicals that undergo oxidative reactions quickly in the medium. After that, Fe^{3+} is generated back through PS activation. So, SRs are produced and effectively degrade SMX through oxidative mechanisms yielding less stable molecules potent to further transformation. Furthermore, in the presence of UVA irradiation, $\equiv Fe^{3+}$ undergo photochemical conversion into Fe^{2+} (Eq.17) on the surface of MIL88-A [98]. As a result, HRs are produced attack SMX allowing its degradation. This was clearly noticed by the complete degradation of SMX in the UVA/MIL88-A/PS system compared to 12% degradation in the MIL88-A/PS system.

$$S_2O_8^{2-} + 2H_2O \rightarrow 2SO_4^{2-} + HO_2^- + 3H^+ \tag{14}$$

$$S_2O_8^{2-} + HO_2^- \rightarrow SO_4^{2-} + SO_4^{-\bullet} + O_2^{-\bullet} + H^+ \tag{15}$$

$$SO_4^{-\bullet} + H_2O \rightarrow SO_4^{2-} + OH^\bullet + H^+ \tag{16}$$

$$\text{Fe(III)OH}^{2+} + h\sigma \rightarrow \text{Fe(II)} + \text{HO}^\bullet \tag{17}$$
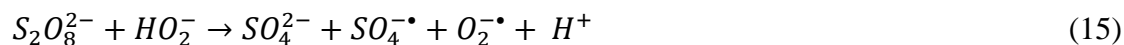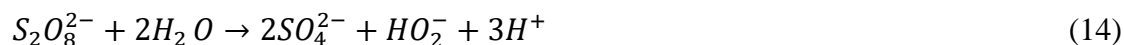
c. Proposed SMX degradation mechanism

In order to get more insight, the SMX removal mechanism, mass spectrometry (MS) was conducted in the present study. It is important to mention that some studies worked on identifying SMX degradation products [34,78,99], however, the results obtained varied from one system to another. In this study SCIEX X500R QTOF was used to detect and identify SMX degradation products in the UVA/MIL88-A/PS/ SMX system. This machine allows accurate determination of the byproducts obtained with the designed structures (error ≤ 2 ppm). In the above mentioned system three byproducts (BP) were obtained and identified by the HPLC and MS analysis. In pathway 1, the sulfonamide moiety was susceptible to an electrophilic attack by OH$^\bullet$ or SO$_4$$^\bullet$ leading to S-N bong cleavage, thus BP1 is formed (m/z = 99) represented in Fig 26. In pathway 2, intermolecular Smiles-type rearrangement of the anilino radical took place by SRs attack through electron transfer mechanism producing SO$_2$ extrusion product (SEP) (m/z = 190) shown in Fig. 27. Finally, in pathway 3, SMX undergoes oxidation to give BP1, specifically SRs and/or HRs attacked N7 of SMX which is the most electronegative nitrogen in SMX structure (m/z = 284) (Fig, 28)..

Table 2. SMX and byproducts identified by MS.

Compound	Molecular formula	ESI mode	m/z	Error (ppm)	R.T. (min)	Proposed structure
SMX	$C_{10}H_{11}N_3O_3S$	Positive	254.0593	-0.3	5.92	
BP1	$C_4H_6ON_2$	Positive	99.055	0.8	2.16	
BP2	$C_{10}H_{11}N_3O$	Positive	190.097	-0.2	5.93	
BP3	$C_{10}H_9O_5N_3S$	Positive	284.034	-1	8.63	
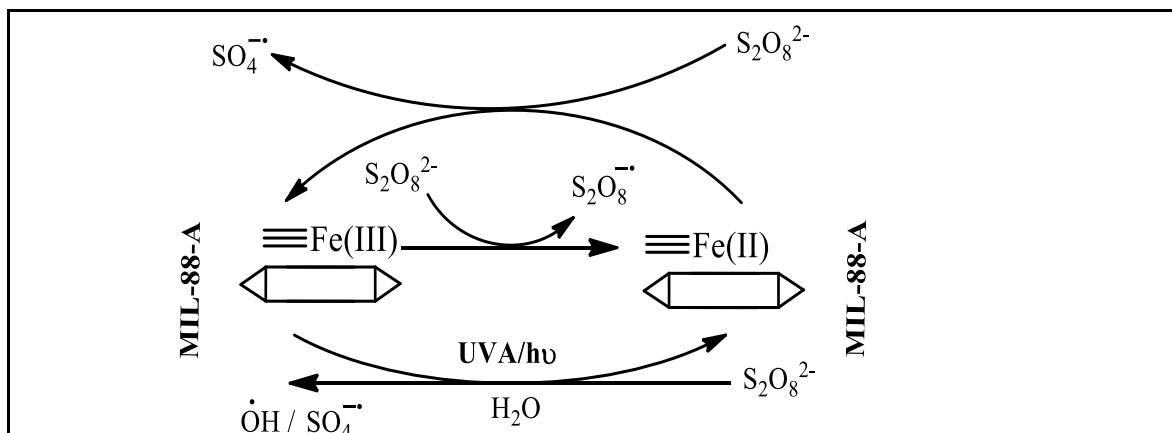
Fig. 29. Activation mechanism of PS in the UVA/MIL88-A system
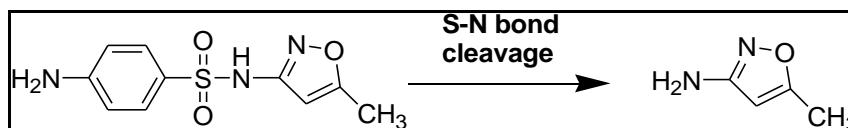
Fig. 30. Formation mechanism of BP1.
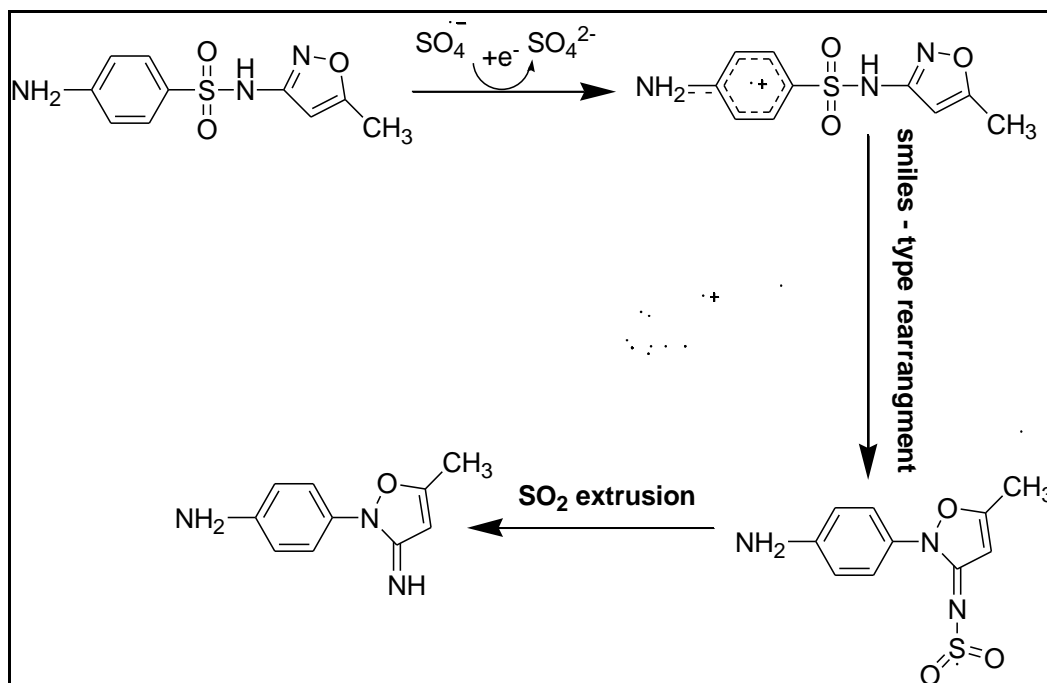
Fig. 31. Formation mechanism of BP2.
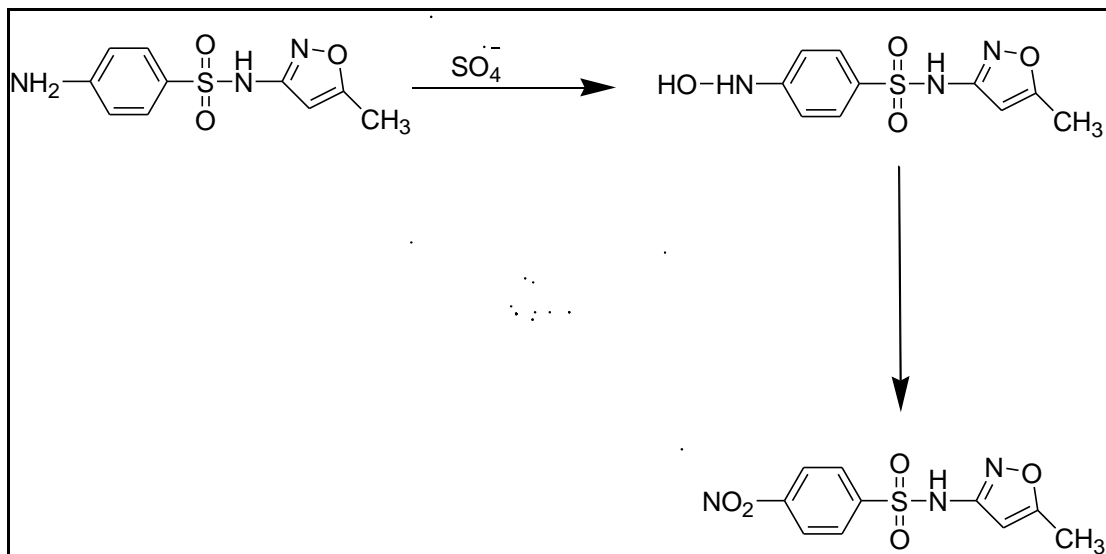
Fig. 32. Formation mechanism of BP3.

60
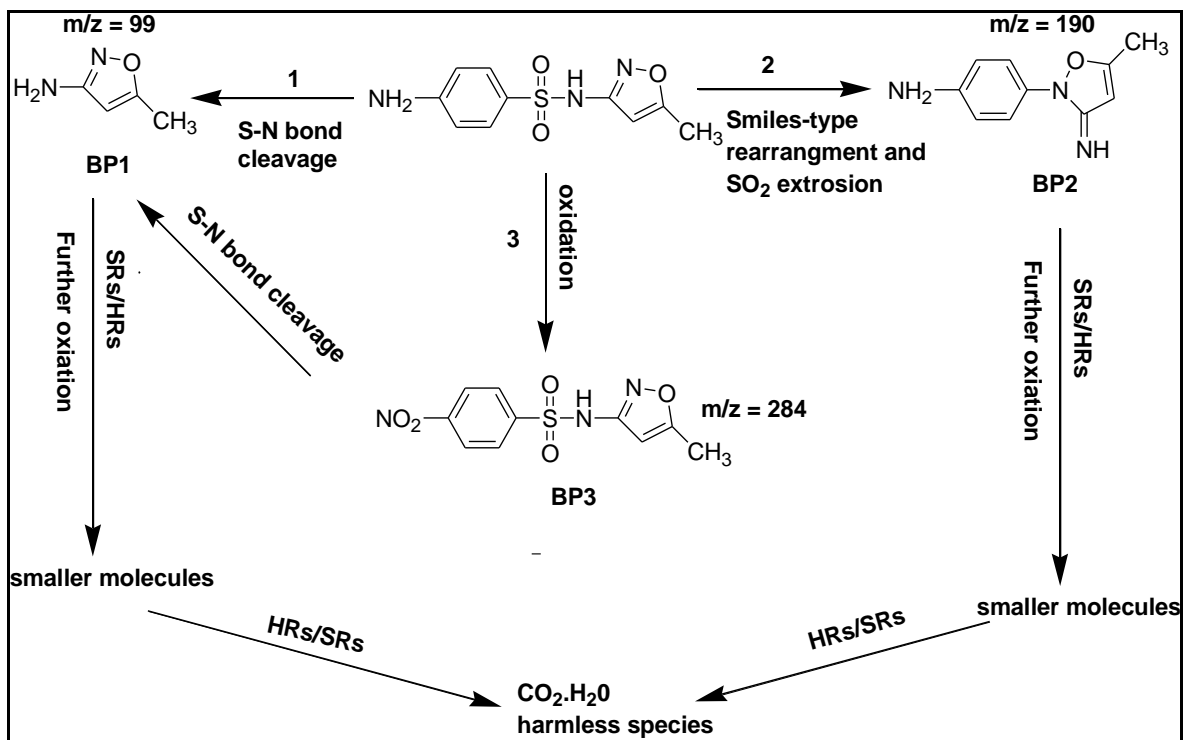
Fig. 33. Overall degradation mechanism of SMX in the UVA/MIL88-A/PS system.

CHAPTER 4

CONCLUSION

In this study, PS- based AOPs proved to be highly efficient in the degradation of hazardous pharmaceuticals like SMX. Herein, a heterogeneous catalyst, MIL88-A was synthesized with the advantage of using low-cost, simple and organic solvent free process. The elimination of SMX was demonstrated in two different systems: UVA/MIL88-A/PS and solar/MIL88-A/PS systems. Several parameters were considered to reach a higher efficiency for the degradation process. [MIL88-A] alone showed no significant effect on the degradation of SMX in the absence and in the presence of irradiation (UVA or solar). The combined effect of UVA or solar /MIL88-A/PS showed promising results, whereby total degradation of SMX was reached within 80 min and 5-20 min in the UVA/MIL88A/PS and solar/MIL88-A/PS systems, respectively. The results also demonstrated that MIL88-A may be used for three successive cycles of activation experiments with PS without showing a decrease in the catalytic activity of the MOF. Moreover, MS analysis were conducted to identify the degradation products of SMX, three different byproducts were identified with the proposed formation mechanism of each. EPR analysis showed the presence of HRs as well as SRs to better understand the activation mechanism of PS on the surface of the MOF. Future directions to consider under this work are the investigation of parameters like the reaction stoichiometric efficiency (RSE) along with the TOC so as to improve the mineralization rate while keeping significant RSE to compete with existing PS-activated AOP systems.

REFERENCES

[1] A.J. Ebele, M.A.-E. Abdallah, S. Harrad, Pharmaceuticals and personal care products (PPCPs) in the freshwater aquatic environment, Emerg. Contam. 3 (2017) 1–16.

[2] J.-L. Liu, M.-H. Wong, Pharmaceuticals and personal care products (PPCPs): a review on environmental contamination in China, Environ. Int. 59 (2013) 208–224.

[3] J.L. Tambosi, L.Y. Yamanaka, H.J. JosÃ\copyright, R. de F.P.M. Moreira, H.F. SchrÃ\Pder, Recent research data on the removal of pharmaceuticals from sewage treatment plants (STP), QuÃ\-Mica Nov. 33 (2010) 411–420.

[4] S. Mompelat, B. Le Bot, O. Thomas, Occurrence and fate of pharmaceutical products and by-products, from resource to drinking water, Environ. Int. 35 (2009) 803–814.

[5] P. Bottoni, S. Caroli, A.B. Caracciolo, Pharmaceuticals as priority water contaminants, Toxicol. Environ. Chem. 92 (2010) 549–565. https://doi.org/10.1080/02772241003614320.

[6] K.E. Arnold, A.R. Brown, G.T. Ankley, J.P. Sumpter, Medicating the environment: assessing risks of pharmaceuticals to wildlife and ecosystems, (2014).

[7] S. Zorita, L. Mårtensson, L. Mathiasson, Occurrence and removal of pharmaceuticals in a municipal sewage treatment system in the south of Sweden, Sci. Total Environ. 407 (2009) 2760–2770.

[8] G.R. Boyd, J.M. Palmeri, S. Zhang, D.A. Grimm, Pharmaceuticals and personal care products (PPCPs) and endocrine disrupting chemicals (EDCs) in stormwater canals and Bayou St. John in New Orleans, Louisiana, USA, Sci. Total Environ. (2004). https://doi.org/10.1016/j.scitotenv.2004.03.018.

[9] D. Ashton, M. Hilton, K. V. Thomas, Investigating the environmental transport of human pharmaceuticals to streams in the United Kingdom, Sci. Total Environ. (2004). https://doi.org/10.1016/j.scitotenv.2004.04.062.

[10] M. Carballa, F. Omil, J.M. Lema, M. Llompart, C. García-Jares, I. Rodríguez, M. Gómez, T. Ternes, Behavior of pharmaceuticals, cosmetics and hormones in a sewage treatment plant, Water Res. (2004). https://doi.org/10.1016/j.watres.2004.03.029.

[11] N. Lindqvist, T. Tuhkanen, L. Kronberg, Occurrence of acidic pharmaceuticals in raw and treated sewages and in receiving waters, Water Res. 39 (2005) 2219–2228.

[12] N. Nakada, T. Tanishima, H. Shinohara, K. Kiri, H. Takada, Pharmaceutical chemicals and endocrine disrupters in municipal wastewater in Tokyo and their removal during activated sludge treatment, Water Res. (2006). https://doi.org/10.1016/j.watres.2006.06.039.

[13] J. Fick, H. Söderström, R.H. Lindberg, C. Phan, M. Tysklind, D.G.J. Larsson, Contamination of surface, ground, and drinking water from pharmaceutical production, Environ. Toxicol. Chem. 28 (2009) 2522–2527.

[14] O. Cardoso, J.-M. Porcher, W. Sanchez, Factory-discharged pharmaceuticals could be a relevant source of aquatic environment contamination: review of evidence and

need for knowledge, Chemosphere. 115 (2014) 20–30.

[15] T. Heberer, Occurrence, fate, and removal of pharmaceutical residues in the aquatic environment: A review of recent research data, Toxicol. Lett. (2002). https://doi.org/10.1016/S0378-4274(02)00041-3.

[16] T.A. Ternes, M. Meisenheimer, D. McDowell, F. Sacher, H.J. Brauch, B. Haist-Gulde, G. Preuss, U. Wilme, N. Zulei-Seibert, Removal of pharmaceuticals during drinking water treatment, Environ. Sci. Technol. (2002). https://doi.org/10.1021/es015757k.

[17] R. Andreozzi, V. Caprio, A. Insola, R. Marotta, Advanced oxidation processes (AOP) for water purification and recovery, Catal. Today. 53 (1999) 51–59.

[18] P.R. Gogate, A.B. Pandit, A review of imperative technologies for wastewater treatment I: oxidation technologies at ambient conditions, Adv. Environ. Res. 8 (2004) 501–551. https://doi.org/https://doi.org/10.1016/S1093-0191(03)00032-7.

[19] C. Wei, F. Zhang, Y. Hu, C. Feng, H. Wu, Ozonation in water treatment: The generation, basic properties of ozone and its practical application, Rev. Chem. Eng. (2017). https://doi.org/10.1515/revce-2016-0008.

[20] S.O. Ganiyu, M. Zhou, C.A. Martínez-Huitle, Heterogeneous electro-Fenton and photoelectro-Fenton processes: A critical review of fundamental principles and application for water/wastewater treatment, Appl. Catal. B Environ. (2018). https://doi.org/10.1016/j.apcatb.2018.04.044.

[21] B.A. Wols, C.H.M. Hofman-Caris, Review of photochemical reaction constants of organic micropollutants required for UV advanced oxidation processes in water, Water Res. (2012). https://doi.org/10.1016/j.watres.2012.03.036.

[22] I.A. Ike, K.G. Linden, J.D. Orbell, M. Duke, Critical review of the science and sustainability of persulphate advanced oxidation processes, Chem. Eng. J. 338 (2018) 651–669. https://doi.org/10.1016/j.cej.2018.01.034.

[23] Y. Zhou, Y. Xiang, Y. He, Y. Yang, J. Zhang, L. Luo, H. Peng, C. Dai, F. Zhu, L. Tang, Applications and factors influencing of the persulfate-based advanced oxidation processes for the remediation of groundwater and soil contaminated with organic compounds, J. Hazard. Mater. 359 (2018) 396–407. https://doi.org/10.1016/j.jhazmat.2018.07.083.

[24] J. Yan, L. Han, W. Gao, S. Xue, M. Chen, Biochar supported nanoscale zerovalent iron composite used as persulfate activator for removing trichloroethylene, Bioresour. Technol. 175 (2015) 269—274. https://doi.org/10.1016/j.biortech.2014.10.103.

[25] W. Ren, Z. Zhou, Y. Zhu, L.-M. Jiang, H. Wei, T. Niu, P. Fu, Z. Qiu, Effect of sulfate radical oxidation on disintegration of waste activated sludge, Int. Biodeterior. Biodegradation. 104 (2015) 384–390.

[26] S. Helmut, Strategies of antioxidant defense, EJB Rev. 1993. 215 (2012) 101.

[27] L.W. Matzek, K.E. Carter, Activated persulfate for organic chemical degradation: A review, Chemosphere. (2016). https://doi.org/10.1016/j.chemosphere.2016.02.055.

[28] A. Ghauch, A.M. Tuqan, N. Kibbi, Ibuprofen removal by heated persulfate in aqueous solution: A kinetics study, Chem. Eng. J. 197 (2012) 483–492. https://doi.org/http://dx.doi.org/10.1016/j.cej.2012.05.051.

[29] A. Ghauch, A.M. Tuqan, N. Kibbi, S. Geryes, Methylene blue discoloration by

heated persulfate in aqueous solution, Chem. Eng. J. 213 (2012) 259–271.

[30] M. Amasha, A. Baalbaki, A. Ghauch, A comparative study of the common persulfate activation techniques for the complete degradation of an NSAID: The case of Ketoprofen, 2018. https://doi.org/10.1016/j.cej.2018.05.118.

[31] M. Amasha, A. Baalbaki, S. Al Hakim, R. El Asmar, A. Ghauch, Degradation of a toxic molecule o-toluidine in industrial effluents using UV254/PS system, J. Adv. Oxid. Technol. 21 (2018) 20170099.

[32] A. Ghauch, A. Baalbaki, M. Amasha, R. El Asmar, O. Tantawi, Contribution of persulfate in UV-254 nm activated systems for complete degradation of chloramphenicol antibiotic in water, Chem. Eng. J. 317 (2017) 1012–1025.

[33] Y. Liu, X. He, Y. Fu, D.D. Dionysiou, Kinetics and mechanism investigation on the destruction of oxytetracycline by UV-254 nm activation of persulfate, J. Hazard. Mater. 305 (2016) 229–239.

[34] A. Ghauch, G. Ayoub, S. Naim, Degradation of sulfamethoxazole by persulfate assisted micrometric Fe0 in aqueous solution, Chem. Eng. J. 228 (2013) 1168–1181.

[35] S. Naim, A. Ghauch, Ranitidine abatement in chemically activated persulfate systems: assessment of industrial iron waste for sustainable applications, Chem. Eng. J. 288 (2016) 276–288.

[36] M.G. Antoniou, Mechanistic studies on the degradation of cyanobacterial toxins and other nitrogen containing compounds with hydroxyl and sulfate radical based Advanced Oxidation Technologies, University of Cincinnati, 2010. http://rave.ohiolink.edu/etdc/view?acc_num=ucin1267460267.

[37] K.-Y.A. Lin, H.-A. Chang, C.-J. Hsu, Iron-based metal organic framework, MIL-88A, as a heterogeneous persulfate catalyst for decolorization of Rhodamine B in water, Rsc Adv. 5 (2015) 32520–32530.

[38] P. Horcajada, R. Gref, T. Baati, P.K. Allan, G. Maurin, P. Couvreur, G. Férey, R.E. Morris, C. Serre, Metal-organic frameworks in biomedicine, Chem. Rev. (2012). https://doi.org/10.1021/cr200256v.

[39] G. Férey, Hybrid porous solids: Past, present, future, Chem. Soc. Rev. (2008). https://doi.org/10.1039/b618320b.

[40] N.A. Khan, Z. Hasan, S.H. Jhung, Adsorptive removal of hazardous materials using metal-organic frameworks (MOFs): A review, J. Hazard. Mater. (2013). https://doi.org/10.1016/j.jhazmat.2012.11.011.

[41] P.Z. Moghadam, A. Li, S.B. Wiggin, A. Tao, A.G.P. Maloney, P.A. Wood, S.C. Ward, D. Fairen-Jimenez, Development of a Cambridge Structural Database Subset: A Collection of Metal-Organic Frameworks for Past, Present, and Future, Chem. Mater. 29 (2017) 2618–2625. https://doi.org/10.1021/acs.chemmater.7b00441.

[42] J. Wang, J. Wan, Y. Ma, Y. Wang, M. Pu, Z. Guan, Metal-organic frameworks MIL-88A with suitable synthesis conditions and optimal dosage for effective catalytic degradation of Orange G through persulfate activation, RSC Adv. (2016). https://doi.org/10.1039/C6RA24429G.

[43] J.-R. Li, Y. Ma, M.C. McCarthy, J. Sculley, J. Yu, H.-K. Jeong, P.B. Balbuena, H.-C. Zhou, Carbon dioxide capture-related gas adsorption and separation in metal-organic frameworks, Coord. Chem. Rev. 255 (2011) 1791–1823.

[44] K. Sumida, D.L. Rogow, J.A. Mason, T.M. McDonald, E.D. Bloch, Z.R. Herm, T.-

H. Bae, J.R. Long, Carbon dioxide capture in metal–organic frameworks, Chem. Rev. 112 (2011) 724–781.

[45] M.P. Suh, H.J. Park, T.K. Prasad, D.-W. Lim, Hydrogen storage in metal–organic frameworks, Chem. Rev. 112 (2011) 782–835.

[46] P. Horcajada, R. Gref, T. Baati, P.K. Allan, G. Maurin, P. Couvreur, G. Ferey, R.E. Morris, C. Serre, Metal–organic frameworks in biomedicine, Chem. Rev. 112 (2011) 1232–1268.

[47] A.C. McKinlay, R.E. Morris, P. Horcajada, G. Férey, R. Gref, P. Couvreur, C. Serre, BioMOFs: Metal-organic frameworks for biological and medical applications, Angew. Chemie - Int. Ed. (2010). https://doi.org/10.1002/anie.201000048.

[48] M. Kurmoo, Magnetic metal-organic frameworks, Chem. Soc. Rev. (2009). https://doi.org/10.1039/b804757j.

[49] T. Uemura, N. Yanai, S. Kitagawa, Polymerization reactions in porous coordination polymers, Chem. Soc. Rev. 38 (2009) 1228–1236.

[50] J. Lee, O.K. Farha, J. Roberts, K.A. Scheidt, S.T. Nguyen, J.T. Hupp, Metal-organic framework materials as catalysts, Chem. Soc. Rev. (2009). https://doi.org/10.1039/b807080f.

[51] E. Haque, J.E. Lee, I.T. Jang, Y.K. Hwang, J.S. Chang, J. Jegal, S.H. Jhung, Adsorptive removal of methyl orange from aqueous solution with metal-organic frameworks, porous chromium-benzenedicarboxylates, J. Hazard. Mater. (2010). https://doi.org/10.1016/j.jhazmat.2010.05.047.

[52] E.Y. Park, Z. Hasan, N.A. Khan, S.H. Jhung, Adsorptive removal of bisphenol-A from water with a metal-organic framework, a porous chromium-benzenedicarboxylate., J. Nanosci. Nanotechnol. (2013).

[53] S. Yuan, L. Feng, K. Wang, J. Pang, M. Bosch, C. Lollar, Y. Sun, J. Qin, X. Yang, P. Zhang, Q. Wang, L. Zou, Y. Zhang, L. Zhang, Y. Fang, J. Li, H.C. Zhou, Stable Metal–Organic Frameworks: Design, Synthesis, and Applications, Adv. Mater. (2018). https://doi.org/10.1002/adma.201704303.

[54] A.D. Paine, A. J., Dayan, Mechanisms of chromium toxicity, carcinogenicity and allergenicity: Review of the literature from 1985 to 2000, Hum. Exp. Toxicol. (2001). https://doi.org/10.1191/096032701682693062.

[55] M. Özcan, A. Allahbeickaraghi, M. Dündar, Possible hazardous effects of hydrofluoric acid and recommendations for treatment approach: A review, Clin. Oral Investig. (2012). https://doi.org/10.1007/s00784-011-0636-6.

[56] M. Tong, D. Liu, Q. Yang, S. Devautour-Vinot, G. Maurin, C. Zhong, Influence of framework metal ions on the dye capture behavior of MIL-100 (Fe, Cr) MOF type solids, J. Mater. Chem. A. (2013). https://doi.org/10.1039/c3ta11807j.

[57] S.H. Huo, X.P. Yan, Metal-organic framework MIL-100(Fe) for the adsorption of malachite green from aqueous solution, J. Mater. Chem. (2012). https://doi.org/10.1039/c2jm16513a.

[58] Z. Hasan, J. Jeon, S.H. Jhung, Adsorptive removal of naproxen and clofibric acid from water using metal-organic frameworks, J. Hazard. Mater. (2012). https://doi.org/10.1016/j.jhazmat.2012.01.005.

[59] T.A. Vu, G.H. Le, C.D. Dao, L.Q. Dang, K.T. Nguyen, Q.K. Nguyen, P.T. Dang, H.T.K. Tran, Q.T. Duong, T. V. Nguyen, G.D. Lee, Arsenic removal from aqueous

solutions by adsorption using novel MIL-53(Fe) as a highly efficient adsorbent, RSC Adv. (2015). https://doi.org/10.1039/c4ra12326c.

[60] Y. Gao, K. Liu, R. Kang, J. Xia, G. Yu, S. Deng, A comparative study of rigid and flexible MOFs for the adsorption of pharmaceuticals: kinetics, isotherms and mechanisms, J. Hazard. Mater. 359 (2018) 248–257.

[61] F. Ke, L.-G. Qiu, Y.-P. Yuan, F.-M. Peng, X. Jiang, A.-J. Xie, Y.-H. Shen, J.-F. Zhu, Thiol-functionalization of metal-organic framework by a facile coordination-based postsynthetic strategy and enhanced removal of Hg2+ from water, J. Hazard. Mater. 196 (2011) 36–43.

[62] J. Wang, J. Wan, Y. Ma, Y. Wang, M. Pu, Z. Guan, Metal-organic frameworks MIL-88A with suitable synthesis conditions and optimal dosage for effective catalytic degradation of Orange G through persulfate activation, RSC Adv. (2016). https://doi.org/10.1039/C6RA24429G.

[63] X. Li, W. Guo, Z. Liu, R. Wang, H. Liu, Fe-based MOFs for efficient adsorption and degradation of acid orange 7 in aqueous solution via persulfate activation, Appl. Surf. Sci. 369 (2016) 130–136. https://doi.org/10.1016/j.apsusc.2016.02.037.

[64] H. Hu, H. Zhang, Y. Chen, Y. Chen, L. Zhuang, H. Ou, Enhanced photocatalysis degradation of organophosphorus flame retardant using MIL-101(Fe)/persulfate: Effect of irradiation wavelength and real water matrixes, Chem. Eng. J. 368 (2019) 273–284. https://doi.org/10.1016/j.cej.2019.02.190.

[65] M. Pu, Z. Guan, Y. Ma, J. Wan, Y. Wang, M.L. Brusseau, H. Chi, Synthesis of iron-based metal-organic framework MIL-53 as an efficient catalyst to activate persulfate for the degradation of Orange G in aqueous solution, Appl. Catal. A Gen. 549 (2018) 82–92. https://doi.org/10.1016/j.apcata.2017.09.021.

[66] H. Li, J. Wan, Y. Ma, Y. Wang, X. Chen, Z. Guan, Degradation of refractory dibutyl phthalate by peroxymonosulfate activated with novel catalysts cobalt metal-organic frameworks: Mechanism, performance, and stability, J. Hazard. Mater. 318 (2016) 154–163. https://doi.org/10.1016/j.jhazmat.2016.06.058.

[67] C. Nguyen Dang Giang, Z. Sebesvari, F. Renaud, I. Rosendahl, Q. Hoang Minh, W. Amelung, Occurrence and dissipation of the antibiotics sulfamethoxazole, sulfadiazine, trimethoprim, and enrofloxacin in the Mekong Delta, Vietnam, PLoS One. 10 (2015) e0131855.

[68] J.C. Underwood, R.W. Harvey, D.W. Metge, D.A. Repert, L.K. Baumgartner, R.L. Smith, T.M. Roane, L.B. Barber, Effects of the antimicrobial sulfamethoxazole on groundwater bacterial enrichment, Environ. Sci. Technol. 45 (2011) 3096–3101.

[69] B.A. Wilson, V.H. Smith, F. deNoyelles, C.K. Larive, Effects of three pharmaceutical and personal care products on natural freshwater algal assemblages, Environ. Sci. Technol. 37 (2003) 1713–1719.

[70] C.W. Knapp, C.A. Engemann, M.L. Hanson, P.L. Keen, K.J. Hall, D.W. Graham, Indirect evidence of transposon-mediated selection of antibiotic resistance genes in aquatic systems at low-level oxytetracycline exposures, Environ. Sci. Technol. 42 (2008) 5348–5353.

[71] M.C. Dodd, C.-H. Huang, Transformation of the antibacterial agent sulfamethoxazole in reactions with chlorine: kinetics, mechanisms, and pathways, Environ. Sci. Technol. 38 (2004) 5607–5615.

[72] R.F. Dantas, S. Contreras, C. Sans, S. Esplugas, Sulfamethoxazole abatement by means of ozonation, J. Hazard. Mater. 150 (2008) 790–794.

[73] M. Petrovic, D. Barceló, LC-MS for identifying photodegradation products of pharmaceuticals in the environment, TrAC Trends Anal. Chem. 26 (2007) 486–493.

[74] A.G. Trovó, R.F.P. Nogueira, A. Agüera, C. Sirtori, A.R. Fernández-Alba, Photodegradation of sulfamethoxazole in various aqueous media: persistence, toxicity and photoproducts assessment, Chemosphere. 77 (2009) 1292–1298.

[75] M.N. Abellán, B. Bayarri, J. Giménez, J. Costa, Photocatalytic degradation of sulfamethoxazole in aqueous suspension of TiO2, Appl. Catal. B Environ. 74 (2007) 233–241.

[76] M.N. Abellán, J. Giménez, S. Esplugas, Photocatalytic degradation of antibiotics: the case of sulfamethoxazole and trimethoprim, Catal. Today. 144 (2009) 131–136.

[77] D. Klauson, M. Krichevskaya, M. Borissova, S. Preis, Aqueous photocatalytic oxidation of sulfamethizole, Environ. Technol. 31 (2010) 1547–1555.

[78] G. Ayoub, A. Ghauch, Assessment of bimetallic and trimetallic iron-based systems for persulfate activation: application to sulfamethoxazole degradation, Chem. Eng. J. 256 (2014) 280–292.

[79] S. Bhattacharjee, J.-S. Choi, S.-T. Yang, S.B. Choi, J. Kim, W.-S. Ahn, Solvothermal Synthesis of Fe-MOF-74 and Its Catalytic Properties in Phenol Hydroxylation, J. Nanosci. Nanotechnol. 10 (2010) 135–141. https://doi.org/10.1166/jnn.2010.1493.

[80] T. Chalati, P. Horcajada, R. Gref, P. Couvreur, C. Serre, Optimisation of the synthesis of MOF nanoparticles made of flexible porous iron fumarate MIL-88A, J. Mater. Chem. (2011). https://doi.org/10.1039/c0jm03563g.

[81] G. Ferraresi, C. Villevieille, I. Czekaj, M. Horisberger, P. Novák, M. El Kazzi, SnO2 model electrode cycled in Li-ion battery reveals the formation of Li2SnO3 and Li8SnO6 phases through conversion reactions, ACS Appl. Mater. Interfaces. 10 (2018) 8712–8720.

[82] A. Baalbaki, N. Zein Eddine, S. Jaber, M. Amasha, A. Ghauch, Rapid quantification of persulfate in aqueous systems using a modified HPLC unit, Talanta. 178 (2018) 237–245. https://doi.org/10.1016/j.talanta.2017.09.036.

[83] K.Y. Andrew Lin, H.A. Chang, C.J. Hsu, Iron-based metal organic framework, MIL-88A, as a heterogeneous persulfate catalyst for decolorization of Rhodamine B in water, RSC Adv. (2015). https://doi.org/10.1039/c5ra01447f.

[84] E.Y. Ionashiro, F.J. Caires, A.B. Siqueira, L.S. Lima, C.T. Carvalho, Thermal behaviour of fumaric acid, sodium fumarate and its compounds with light trivalent lanthanides in air atmosphere, J. Therm. Anal. Calorim. 108 (2012) 1183–1188.

[85] R. El Asmar, A. Baalbaki, Z. Abou Khalil, S. Naim, A. Bejjani, A. Ghauch, Iron-based metal organic framework MIL-88-A for the degradation of naproxen in water through persulfate activation, Chem. Eng. J. 405 (2021) 126701.

[86] W. Huang, C. Jing, X. Zhang, M. Tang, L. Tang, M. Wu, N. Liu, Integration of plasmonic effect into spindle-shaped MIL-88A (Fe): Steering charge flow for enhanced visible-light photocatalytic degradation of ibuprofen, Chem. Eng. J. 349 (2018) 603–612.

[87] J.M. Monteagudo, A. Durán, R. Culebradas, I. San Martín, A. Carnicer,

Optimization of pharmaceutical wastewater treatment by solar/ferrioxalate photo-catalysis, J. Environ. Manage. 128 (2013) 210–219.

[88] H.A. Gorrell, Classification of formation waters based on sodium chloride content, Am. Assoc. Pet. Geol. Bull. 42 (1958) 2513.

[89] S. Al Hakim, S. Jaber, N.Z. Eddine, A. Baalbaki, A. Ghauch, Degradation of theophylline in a UV254/PS system: Matrix effect and application to a factory effluent, Chem. Eng. J. 380 (2020) 122478.

[90] Z. Wei, F.A. Villamena, L.K. Weavers, Kinetics and mechanism of ultrasonic activation of persulfate: an in situ EPR spin trapping study, Environ. Sci. Technol. 51 (2017) 3410–3417.

[91] Y. Liu, X. Chen, Y. Yang, Y. Feng, D. Wu, S. Mao, Activation of persulfate with metal–organic framework-derived nitrogen-doped porous Co@ C nanoboxes for highly efficient p-Chloroaniline removal, Chem. Eng. J. 358 (2019) 408–418.

[92] X. Duan, C. Su, J. Miao, Y. Zhong, Z. Shao, S. Wang, H. Sun, Insights into perovskite-catalyzed peroxymonosulfate activation: maneuverable cobalt sites for promoted evolution of sulfate radicals, Appl. Catal. B Environ. 220 (2018) 626–634.

[93] S. Stoll, A. Schweiger, EasySpin, a comprehensive software package for spectral simulation and analysis in EPR, J. Magn. Reson. 178 (2006) 42–55.

[94] M.J. Davies, B.C. Gilbert, J.K. Stell, A.C. Whitwood, Nucleophilic substitution reactions of spin adducts. Implications for the correct identification of reaction intermediates by EPR/spin trapping, J. Chem. Soc. Perkin Trans. 2. (1992) 333–335.

[95] H. Liu, T.A. Bruton, F.M. Doyle, D.L. Sedlak, In situ chemical oxidation of contaminated groundwater by persulfate: Decomposition by Fe(III)- and Mn(IV)-containing oxides and aquifer materials, Environ. Sci. Technol. (2014). https://doi.org/10.1021/es502056d.

[96] Y. Gao, S.A. Chambers, Heteroepitaxial growth of α-Fe2O3, γ-Fe2O3 and Fe3O4 thin films by oxygen-plasma-assisted molecular beam epitaxy, J. Cryst. Growth. 174 (1997) 446–454.

[97] H. Bao, X. Chen, J. Fang, Z. Jiang, W. Huang, Structure-activity relation of Fe 2 O 3–CeO 2 composite catalysts in CO oxidation, Catal. Letters. 125 (2008) 160–167.

[98] C.Y. Kwan, W. Chu, Photodegradation of 2, 4-dichlorophenoxyacetic acid in various iron-mediated oxidation systems, Water Res. 37 (2003) 4405–4412.

[99] T. Luo, J. Wan, Y. Ma, Y. Wang, Y. Wan, Sulfamethoxazole degradation by an Fe (ii)-activated persulfate process: insight into the reactive sites, product identification and degradation pathways, Environ. Sci. Process. Impacts. 21 (2019) 1560–1569.